Investigating the relationship between amphotericin B and extracellular vesicles produced by *Streptomyces nodosus*

By Samuel John King

A thesis submitted in partial fulfilment of the requirements for the degree of Master of Research

School of Science and Health

Western Sydney University

2017

Acknowledgements

A big thank you to the following people who have helped me throughout this project:

Jo, for all of your support over the last two years;

Ric, Tim, Shamilla and Sue for assistance with electron microscope operation;

Renee for guidance with phylogenetics;

Greg, Herbert and Adam for technical support;

and Mum, you're the real MVP.

I acknowledge the services of AGRF for sequencing of 16S rDNA products of *Streptomyces "purple"*.

Statement of Authentication

The work presented in this thesis is, to the best of my knowledge and belief, original except as acknowledged in the text. I hereby declare that I have not submitted this material, either in full or in part, for a degree at this or any other institution.

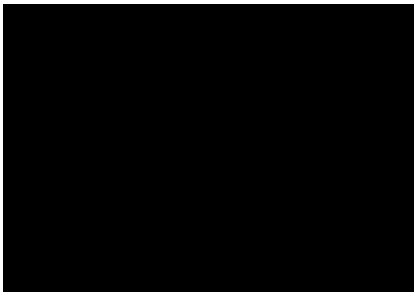

…… (Signature)

Contents

List of Tables

List of Figures

Abbreviations

16S rDNA – DNA sequence coding for the 16S RNA subunit

EtBr – Ethidium bromide

EVs - Extracellular vesicles

TEM - Transmission Electron Microscopy

STEM - Scanning Transmission Electron Microscopy

PKS – Polyketide synthase

Abstract

The antifungal drug amphotericin B is made by *Streptomyces nodosus* and is released into culture broths at concentrations exceeding its solubility in water. The recent discovery of extracellular vesicles derived from *Streptomyces* species suggests that amphotericin B could be released from the biomass using this delivery system. This thesis identified a *Streptomyces* soil isolate through the construction of a phylogenetic tree based on 16S sequences. The soil isolate was used to develop methods to image *Streptomyces* extracellular vesicles using STEM, which were then used to examine whether *S. nodosus* produces extracellular vesicles. Initial co-localisation experiments using size fractionation indicated that amphotericin B was associated with fractions containing extracellular vesicles. Extracellular vesicles from the culture fluid of a mutant unable to produce amphotericin B, indicated that vesicle production was not dependent on amphotericin synthesis but may play a role in delivering other hydrophobic molecules.

CHAPTER 1

INTRODUCTION

1.1 The antifungal drug amphotericin B

Antifungal drugs are used to treat a variety of fungal pathogens from superficial infections estimated to affect 25% of the human population (Havlickova et al 2008), to systemic mycoses occurring primarily in juvenile, elderly and immunocomprimised individuals (Richardson 2005). For systemic infections, three classes of drugs have been effective, polyenes, echinocandins and azoles (Roemer & Krysan 2014). Poor prognosis for patients with various systemic mycoses such as invasive candidiasis (Kullberg & Maiken 2015) and invasive aspergillosis (Taccone et al 2014) highlight the need to develop more effective treatments (Souza & Amaral 2017). As the discovery of new antifungals has been slow over the last 50 years, it may be more feasible to improve drug delivery of current antifungal medicines than to discover new ones. The antifungal with the broadest spectrum for treating systemic fungal infections is the polyene macrolide antibiotic, amphotericin B, which has been used in medical practice for over 50 years (Bartner et al 1957). The broad spectrum of this drug despite side effects and its continued effectiveness after more than a half-century of clinical use, means that improvements of its delivery may improve its tolerance and outcomes for patients with various systemic fungal infections for years to come.

Amphotericin B is a natural product produced by *Streptomyces nodosus*. The amphotericin B molecule has a mycosamine group attached to a 38 membered ring that has seven conjugated double bonds and multiple electronegative hydroxyl groups (Fig. 1.1). The amphotericin B molecule has characteristic wavelengths detectable by UV-Vis spectrophotometry (McNamara et al 1998, Singh et al 2014).

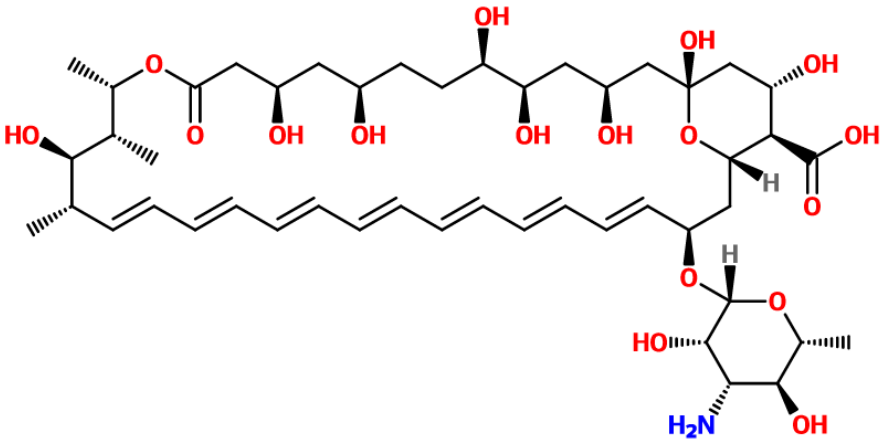

Figure 1.1 The macrolide structure of amphotericin B. The molecular structure of amphotericin B showing a large macrocyclic polyene lactone ring attached to a sugar.

Amphotericin B is produced via a type I polyketide synthase (PKS) system (Caffrey et al 2001, Chuck et al 2006). Multifunctional proteins drive the sequential condensation of three propionate and sixteen acetate units to form an intermediate polyketide ring that is modified by cytochrome P450 and glycosyl transferase enzymes to yield amphotericin B (Caffrey et al 2001). The role of PKS genes for amphotericin B biosynthesis was confirmed in our laboratory by disrupting one of the PKS genes with a hygromycin resistance cassete to create the knockout mutant, *S. nodosus* MAΩ*hyg*, that does not produce amphotericin B (Nikodinovic 2004, Pereira et al 2008).

There are several models to explain the mode of action amphotericin B in fungal membranes. The classical model is via the formation of ion channels. In this model, aggregates of amphotericin B bind to ergosterol in the fungal lipid membrane

creating an electronegative pore through which essential K^+ ions are lost leading to destruction of the organism (Mouri et al 2008). Other models have been proposed including a surface adsorption model and a sterol sponge model (Anderson et al 2014).

IN clinical use in humans amphotericin B can have severe side effects. The macrolide polyene structure of amphotericin B is poorly soluble in water, and in aqueous media can readily form micelles which are problematic for drug delivery (Kawabata et al 2001). While having a higher affinity for ergosterols in fungal membranes, amphotericin B also binds to cholesterol in human cells, which is thought to contribute to the high rates of nephrotoxicity (Kamiński 2014). Some work has been done on producing synthetic analogues with reduced affinity for binding with cholesterol, such as C2' deoxyamphotericin B (Wilcock et al 2013). Improvements in the solubility and delivery of amphotericin B have also been achieved through the use of liposomes.

Liposomes are artificial vesicles, phospholipid membranes containing molecular cargo, used in the delivery of hydrophobic drugs. A liposomal formulation of amphotericin B called AmBisome improves the solubility of amphotericin B and causes reduced rates of nephrotoxicity compared to traditional formulations (Adler-Moore 1994). Amphotericin B co-localises with the vesicle membrane of AmBisome and has also been shown to co-localise with the vesicle membrane of giant unilammelar liposomes (Grudzinski et al 2016). The association of amphotericin B with phospholipid membranes suggests a similar phenomenon may occur within the phospholipid membranes of extracellular vesicles (EVs) produced by *S. nodosus*.

1.2 Natural extracellular vesicles

Organisms across the three domains of life produce EVs (Deatherage & Cookson 2012) and utilise them for diverse processes including predation of microbial competitors (Evan et al 2012), communication (Mashburn & Whitely 2005, Tashiro et al 2010), transport of nucleic acids (Blesa & Berenguer 2015, Das & Halushka 2015) and the delivery of toxins into the extracellular environment (Prangishvili et al 2000). EVs may also function to protect molecules from oxidation as seen in *Frankia sp.* (Ghodhbane-Gtari et al 2014).

Natural EVs have potential in the delivery of therapeutic molecules (Meel et al 2014) and have successfully been used as novel vehicles for therapeutic drug delivery of nucleic acids (Andaloussi et al 2013). As *Streptomyces* have adapted for life in the soil alongside fungi, an EV delivery system of amphotericin B may preferentially target mycotic infections over human cells, reducing side effects and leading to improved patient outcomes. There is currently a lack of evidence demonstrating that *S. nodosus* produces EVs, although other *Streptomyces* species have been shown to produce EVs that are packed with polyketide antibiotics (Schrempf et al 2011, Schrempf & Merling 2015).

For many years it had been noted that some *Streptomyces* develop droplets on the surface of hydrophobic aerial hyphae on solid culture. Recently it was shown that *S. coelicolor* produced droplets containing high quantities of EVs with high protein content (~1 to 2 $\mu g\ \mu L^{-1}$) and densely packed with molecules for secretion including the polyketide antibiotic, actinorhodin (Schrempf et al 2011). Similarly, droplets that

form on the surface of *S. lividans* cultures also are a rich source of EVs that package the polyketide antibiotic undecylprodigiosin and have high protein content (~1 to 2 μg μL^{-1}) (Schrempf & Merling 2015). The discovery of EVs in droplet exudates produced by *S. coelicolor* and *S. lividans* suggests that droplets produced by other *Streptomyces* species may also be novel sources of *Streptomyces* EVs. Unfortunately, *S. nodosus* does not produce droplets on solid media. This means to investigate delivery mechanisms, alternate methods need to be used to isolate EVs from liquid media. EVs from this source are expected to be more dilute than EVs in droplets. Size fractionation techniques have been used to isolate EVs from culture broth of Gram positive organisms (Chutkan et al 2013) and could be employed to isolate *S. nodosus* EVs.

Image analysis is important for the characterisation of EVs . EVs from *S. coelicolor* and *S. lividans* discussed previously were imaged with TEM. TEM is a common technique for imaging EVs in other organisms and samples are often treated with a negative stain, like phosphotungstic acid or osmium tetroxide (Mielańczyk et al 2015). As TEM facilities were not available at the university other techniques were considered. An alternative technique to TEM for the imaging of EVs was scanning transmission electron microscopy (STEM), which was readily available at the university. While STEM has been used to image EVs (Burlaud-Gaillard et al 2014) use of the technique for imaging EVs is not well known and was not included in a recent review of the techniques available for EV detection and characterisation (Nawaz et al 2014).

1.3 Aims

This research aimed to gain insights into the role of *S. nodosus* EVs for amphotericin B delivery once image techniques were developed. A previously unidentified *Streptomyces* strain, *S. "purple"*, was used as a reproducible source of vesicles for this endeavour and was identified as part of this project. These techniques were used to show *S. nodosus* produces EVs. For STEM analysis, EVs were isolated from *S. nodosus* culture broth using size fractionation techniques. TEM facilities at Macquarie University were also used to image *S. nodosus* EVs and comparisons between the TEM and STEM micrographs used to assess the suitability of STEM for imaging EVs. STEM was also used to analyse *S. nodosus* MAΩ*hyg* culture broth extracts for EVs to determine whether the mutant produced EVs. Later stages of the project indicated co-localisation of amphotericin B with *S. nodosus* EVs by UV-Vis spectroscopy and STEM analysis.

CHAPTER 2

MATERIALS AND METHODS

2.1 Materials

2.1.1 Bacterial strains

Streptomyces nodosus wildtype (ATCC 14899) was obtained American Type Culture Collection and maintained as spore suspensions in 20% (v/v) glycerol held at -80 °C. *S. nodosus* MAΩ*hyg*, a mutant strain that does not produce amphotericin B, was made previously in our lab (Nikodinovic 2004, Pereira et al 2008) and maintained as 20% (v/v) glycerol spore suspensions held at -20 °C. The uncharacterised strain designated *S. "purple"* was isolated previously by our group from soil gathered from Western Sydney University's North Parramatta campus (Chuck, unpublished data) and maintained as spore suspensions in H_2O at -20 °C.

2.1.2 Reagents and media components

Bacteriological Agar, Yeast Extract and Malt Extract were from Oxoid. Glycerol, L-asparagine and α-D-glucose were purchased from Sigma-Aldrich. Salts ($K_2HPO_4.3H_2O$, $FeSO_4.7H_2O$, $MnCl_2.4H_2O$, $ZnSO_4.7H_2O$) were from Univar.

Primers for the amplification of the *Streptomyces* 16S RNA sequence *16Sforwhole* (5' GGGAAGCTTCACGGAGAGTTTGATCCT 3') and *16Srevwhole* (5' CCCTCTAGAAAGGAGGTGATCCAGC 3') were synthesised by Sigma-Genosys and had been designed previously using conserved regions of rDNA in the *S. ambofaciens* sequence (Pernodet et al 1989).

2.2 Growth of *Streptomyces* cultures

2.2.1 Growth *S. "purple"* on solid media

Glycerol-asparagine agar (GA) (20 g L^{-1} bacteriological agar, 10 g L^{-1} glycerol, 1.3 g L^{-1} $K_2HPO_4.3H_2O$, 1 g L^{-1} L-asparagine, 10 mg L^{-1} $FeSO_4.7H_2O$, 10 mg L^{-1} $ZnSO_4.7H_2O$, 10 mg L^{-1}, $MnCl_2.4H_2O$) (Shirling and Gottlieb 1966) was used for the growth of *S. "purple"* on solid media. Spore suspensions of *S. "purple"* (1 µL) were germinated on GA agar at 30 °C for 7 days after which mycelial growth with sporulation was evident. Spores of the organism were subcultured onto GA agar and incubated at 30 °C for 3 days until droplets were visible by the naked eye on the surface of the biomass.

2.2.2 Growth of *Streptomyces* strains in liquid media

Growth of *S. "purple"* and *S. nodosus* strains in liquid media were carried out in 250 mL or 1 L baffled flasks containing 30 mL or 125 mL yeast malt glucose (YMG) liquid broth (4 g L^{-1} yeast extract, 10 g L^{-1} malt extract, 4 g L^{-1} α-D-glucose), respectively. Spore suspensions (50-100 µL) of the *Streptomyces* strains were used to inoculate the liquid media and cultivated with shaking (200 rpm) at 30 °C for 3-10 days.

2.3 Identification of the soil derived *S. "purple"*

2.3.1 Isolation of *S. "purple"* gDNA

The isolation of gDNA from *S. "purple"* was performed following methods previously developed by our research group (Nikodinovic et al 2003). *Streptomyces*

"purple" spore suspension (50 µL) was used to inoculate baffled flasks containing YMG liquid media and incubated for 4 days as described in section 2.2.2. The culture biomass was harvested by removal of the supernatant after centrifugation (4500x *g*, 25 °C, 10 min). The pellets were resuspended in lysis solution (10 mL, 0.3 M sucrose, 25 mM EDTA, 25 mM Tris-HCl, 4 U RNase, pH 7.3). Lysozyme (10 mg), and achromopeptidase (5 mg) were added before incubating (37 °C, 20 min). SDS (1 mL, 10% w/v) and proteinase K (5 mg) were added before further incubation with shaking (55 °C, 150 rpm, 90 min). NaCl (3.6 mL, 5 M) and chloroform (15 mL) were added to the tubes before rotating them end over end (20 min). The aqueous phase of the samples was transferred to clean tubes after centrifugation (4500x *g*, 25 °C, 30 min). DNA was precipitated from the aqueous phase by addition of isopropyl alcohol (1 volume) before centrifugation (4500x *g*, 25 °C, 30 min). The supernatant was removed leaving a DNA pellet, to which ethanol was added (1 mL, 70% w/v, 1 min). The ethanol was removed and the DNA pellet allowed to air dry (1 h) before dissolving in DNA buffer (100-200 µL, 60 °C, 10 mM Tris HCl, 10 mM EDTA, pH 7.4) and storing in the freezer (-20 °C).

The sizes of gDNA were investigated with electrophoresis and nucleic acid concentration and DNA purity was quantitated using UV-Vis spectrophotometry as described in section 2.3.3. gDNA previously isolated from *S. neyagawaensis* was available in our lab and was loaded on the gel for size comparison.

2.3.2 Polymerase chain reaction

Polymerase chain reaction (PCR) was performed using the isolated gDNA of *S. "purple"* as a template to amplify the 16S rDNA using the primers *16Sforwhole* and *16Srevwhole*. Reactions contained 10 pmol of each primer, 5 ng template DNA, 12.5 µL AmpliTaq Gold® 360 Master Mix (Invitrogen), 0-5 µL GC enhancer (Invitrogen), and water to a total volume of 25 µL. PCR conditions were 97 °C for 30 s (denaturation), 50 °C for 1 min (annealing) and 72 °C for 1 min (extension) for 30 cycles using a PTC-100 Programmable Thermal Controller (MJ Research Inc.). PCR products were analysed and purified as described in section 2.3.3.

2.3.3 DNA analysis and purification

DNA was separated by electrophoresis (70 V, 1 h) on agarose gels (1% (w/v) in 1 x TAE) using 1 x TAE running buffer containing 0.5 mg L^{-1} EtBr. Gels were visualised by UV light using a Gel Doc EZ-Imager (BioRad). All DNA quantitation was performed using a NanoDrop 2000C UV-Vis spectrophotometer (ThermoScientific). A Purelink Quick Gel Extraction & PCR Purification Combo Kit (Invitrogen) was used to extract and purify 16S PCR products excised from a 1% (w/v) agarose gel in TAE. Purified PCR products were visualised and quantitated as described above. The Australian Genomic Research Facility's (Westmead, Australia) Sanger sequencing service was used for sequencing of the purified PCR products from *S. "purple"* with either primer *16Sforwhole* or *16Srevwhole*.

2.3.4 Bioinformatic analysis of sequenced DNA

Unreliable base reads in the raw forward and reverse 16S rDNA sequences of *S. "purple"* (Appendix 1) were coded as missing data. Combined forward and reverse read length of the *S. "purple"* sequences were shorter than other 16S rDNA sequences of *Streptomyces*, therefore these were aligned to other 16S rDNA sequences with a segment of missing data between the forward and reverse. The DeNovo assembly tool in Geneious software was used to generate a 1454 bp 16S rDNA sequence of *S. "purple"* by inserting N nucleotides between the aligned forward and reverse sequences of *S. "purple"* (Appendix 2). The *S. "purple"* 16S sequence was aligned with 16S sequences of the 115 *Streptomyces* species, 2 *Kitasatospora* species and *Mycobacterium tuberculosis* (Appendix 3), which was added as an out-group. A maximum likelihood phylogeny was generated using IQ-Tree (Nguyen et al 2015) using the ultrafast bootstrap approximation (Minh et al 2013) with 1000 resamplings.

2.4 Imaging *Streptomyces* extracellular vesicles

2.4.1 Isolation of samples for EM analysis

Streptomyces "purple" was grown on solid medium as outlined in section 2.2.1. Droplet exudates that formed on subcultured colonies were collected by placing the copper side of carbon coated copper TEM grids (300 mesh, ProSciTech) to the surface of the droplets. Samples were processed as outlined in section 2.4.2.

S. nodosus and *S. nodosus* MAΩ*hyg* were grown in 30 mL YMG media for 7 days as outlined in section 2.2.2. Cell debris in the liquid broths was removed via centrifugation (15,000x *g*, 25 °C, 15 min) and the supernatant filtered through a syringe driven 0.22 µm filter unit (Millex). The filtered supernatant was added to a 100 kDa molecular weight cut off centrifugal filter device (Amicon) and centrifuged (7500x *g*, 25 °C, 20 min). The filtrate (<100 kDa) of *S. nodosus* was collected and set aside for preparation on TEM grids as a control. The filter devices were inverted and centrifuged (1000x g, 25 °C, 2 min) into a recovery tube to collect the >100 kDa fraction.

2.4.2 Sample preparation for EM imaging

The following procedure was conducted in a biosafety cabinet on parafilm. Droplet exudates of *S. "purple"*, the >100 kDa fraction of *S. nodosus* culture broth (2 µL), *S. nodosus* MAΩ*hyg* culture broth (2 µL), and the <100 kDa filtrate of *S. nodosus* culture broth (2 µL) were added to the copper side of C coated Cu TEM grids and allowed to stand (5 min) at room temperature. The grids were transferred into glutaraldehyde (3% w/v in phosphate buffer pH 7.2, 200 µL, 15 min) to fix the vesicles. The excess liquid was removed by blotting and the grids were transferred into negative stain, phosphotungstic acid (3% w/v, 300 µL, 1 min). The liquid was removed by blotting and the grids moved into drops of deionised water (200 µL, 5 min). The water was removed by blotting and grids allowed to air dry in the hood (60 min) before being stored in a TEM grid box in preparation for imaging.

2.4.3 EM analysis

The samples on TEM grids were investigated by STEM for the presence and morphology of extracellular vesicles using a JEOL 7001F SEM equipped with a TED detector in STEM mode at the Advanced Materials Characterisation Facility, Western Sydney University. STEM images were taken in bright field using a working distance of 10 mm, a probe current of 0.8 A and an electron beam voltages of 15-30 kV.

The >100 kDa fraction of *S. nodosus* culture broth was imaged as a control using a Phillips CM10 TEM with an Olympus SIS megaview G2 Digital camera at the Microscopy Unit, Macquarie University. TEM images were taken in bright field using an electron voltage of 100 kV.

2.5 UV-Vis spectroscopy of culture fluid extracts of *S. nodosus* strains

2.5.1 Amphotericin B detection in wildtype and mutant *S. nodosus* culture broth extracts

Spore suspensions of *S. nodosus* (50 µL) and *S. nodosus* MAΩ*hyg* (50 µL) were cultivated in either 30 mL or 125 mL of YMG media for 3-10 days as outlined in section 2.2.2. A cell free supernatant was obtained after centrifugation (4500 x *g*, 25 °C, 10 min) and removal of the biomass pellet. Samples were prepared for amphotericin B analysis with the addition of DMSO (1 volume), vortexing (5 min) and centrifugation (4500x *g*, 25 °C, 10 min). The supernatants were diluted 10 fold

with 100% (v/v) methanol and vortexed (1 min) before recording the UV-Vis spectra (250-500 nm) using a Cary-100 series UV-Vis spectrophotometer (Agilent).

2.5.2 Size fractionation and UV-Vis analysis of *S. nodosus* culture broth extracts

In some experiments, wildtype *S. nodosus* culture broths were further clarified by passing the cell-free broths through a 0.22 μM syringe filter unit (Millex) to further remove any remaining biomass. The filtrate (2 mL) was size fractionated into >100 kDa and <100 kDa fractions as described in section 2.4.1. The < 100 kDa fraction and the clarified culture broth it was obtained from were further analysed for the presence of amphotericin B as described in section 2.5.1.

CHAPTER 3

RESULTS

3.1 Taxonomic identification of *S. "purple"*

As there was a need to develop in house methods for imaging vesicles of *Streptomyces* species, a reliable source of concentrated EVs was required. None of the characterised organisms in our laboratory maintained the phenotype for droplet production on repeated subculturing. In contrast, an uncharacterised soil isolate assumed to be a *Streptomyces* strain produced droplets on repeated sub-culture. The organism produced pigments secreted into solid media, had an earthy odour, and colony morphology that undergoes differentiation into sporulating aerial hyphae, all of which are characteristic of *Streptomyces* species. The droplets and pigment secreted by the soil isolate were a striking purple colour when grown on GA agar solid media (Fig. 3.1), and so the isolate was designated the "in-house" name *Streptomyces "purple"*. To ensure the organism belonged to the *Streptomyces* genus, experiments to identify *S. "purple"* taxonomically were undertaken using molecular biology and phylogenetic techniques.

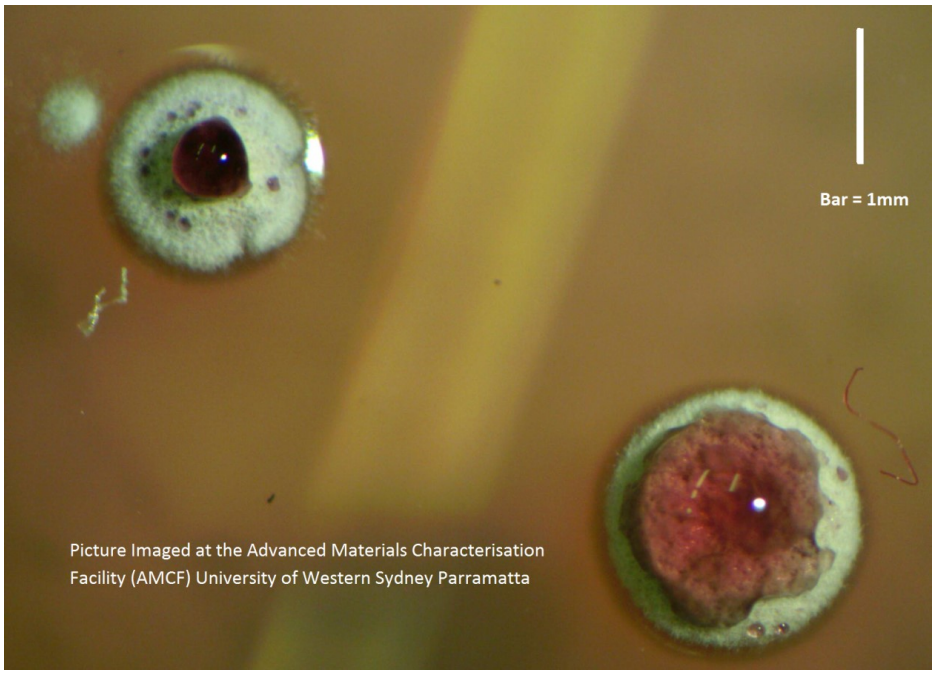

Figure 3.1 Purple droplets on colonies of *S. "purple"*. Scale bar = 1 mm

3.1.1 Isolation of gDNA

gDNA was successfully isolated from *S. "purple"* using methods previously developed by our research group. Agarose gel electrophoresis showed DNA present of sizes >10 kb for the isolated gDNA of *S. "purple"* (Fig. 3.2 Lanes D - H). The size of gDNA products also aligned with a gDNA band from the gDNA of *S. neyagawaensis* (Fig. 3.2 Lane B). The broad, bright bands observed at the bottom of the gel for all of our samples indicated that the samples contained some RNA.

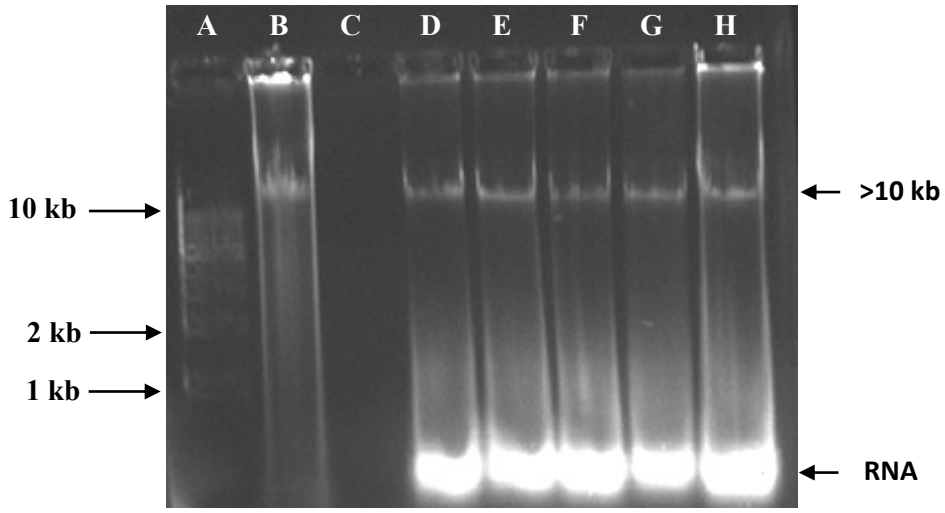

Figure 3.2: Agarose gel electrophoresis of *Streptomyces* gDNA. (Lane A) : 1 kb step ladder (Promega). (Lane B) : gDNA from *S. neyagawaensis*. (Lane C) : DNA isolation buffer. (Lanes D - H) : *S. "purple"* gDNA.

Quantitation via UV-Vis analysis of the gDNA samples showed nucleic acid concentrations ranging from 752 ng μL^{-1} to 3052 ng μL^{-1} (Table 3.1). A260/280 values ranging from 1.82-2.13 indicated samples contained DNA and some RNA.

The sample with an A260/280 value of 1.82 was deemed to have acceptable DNA quality and was used for subsequent PCR reactions.

Table 3.1: A260/280 ratios and concentration of *S. "purple"* gDNA isolates

Sample	Nucleic acid concentration (ng μL^{-1})	A260/280
1	1226	1.82
2	1065	2.10
3	864	2.13
4	752	2.11
5	3052	2.07

3.1.2 PCR

The gDNA isolated from *S. "purple"* was used as template DNA to generate 16S rDNA PCR products for sequencing. PCR products were analysed using electrophoresis with the resulting agarose gel showing 16S PCR products of size ~1.5 kb (Fig. 3.3 Lanes B, C, D, E, G, H). Some minor optimisation showed the PCR reactions containing 10 ng template DNA and no GC enhancer had the brightest bands on the gel (Fig. 3.3 Lanes D, E). In contrast, products of PCR reactions that contained 5 ng template DNA and 0-1 µL GC enhancer produced well defined bands on the gel (Fig. 3.3 Lanes B, C, H, I), while the PCR products of reactions containing 5 ng template DNA and 5 µL GC enhancer showed either no bands (Fig. 3.3 Lane F)

or a very faint band (Fig. 3.3 Lane G). These results indicated that having an increased amount of template DNA was favourable for the PCR reactions.

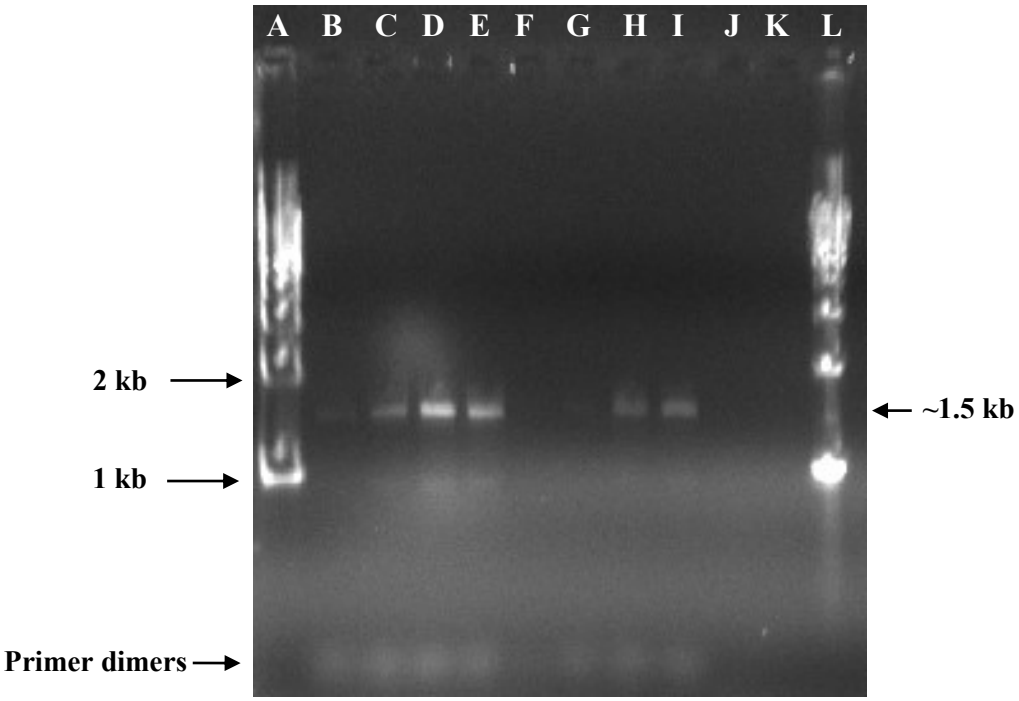

Figure 3.3: Agarose gel of 16S PCR products of *S. "purple"*. (Lanes A and L) : 1kb step ladder (Promega). (Lanes B and C) : Products of PCR containing 0 µL GC enhancer and 5 ng gDNA template showing ~1.5 kb bands. (Lanes D and E) : Products of PCR containing 0 µL GC enhancer and 10 ng gDNA template showing bright ~1.5 kb bands. (Lanes F and G) : Products of PCR containing 5 µL GC enhancer and 5 ng gDNA template showing ~1.5 kb bands. (Lanes H and I): Products of PCR containing 1 µL GC enhancer and 5 ng gDNA template showing ~1.5 kb bands. (Lanes J and K) : Negative controls missing either a forward or reverse primer showing no bands . Primer dimers observed for successful PCR reactions at the end of gel.

The negative controls showed no bands (Fig. 3.3 Lanes J, K) which was expected as the reactions for these products were missing one of either primer *16Sforwhole* or *16Srevwhole*. A broad band at the end of the gel was observed for all successful PCR products, which were suspected to be primer dimers. The resolution of the ladder was fairly poor prompting the purchasing of a new ladder (Fig. 3.3 Lanes A, L).

3.1.3 Gel purification

PCR reactions that showed well defined bands of sizes approx. 1.5 kb were pooled and run on a preparative 1% agarose gel. The 1.5 kb band was purified from the gel and the two resulting samples were checked by electrophoresis and quantitated by UV-Vis analysis.

The purification process was verified by analytical electrophoresis showing very faint bands of sizes ~1.5 kb (Fig. 3.4 Lanes B, C). The negative control (Fig. 3.4 Lane D) had a very faint band from carry over sample that occurred during loading. The unpurified product was also loaded for comparison showing a ~1.5 kb band and a primer dimer band at the end of the gel (Fig. 3.4 Lane E).

PCR products extracted from the preparative gel were quantitated with UV-Vis (Table 3.2). While these products showed no primer dimer bands after electrophoresis (Fig. 3.4 Lanes B, C), their A260/280 ratios were > 2 which indicated they may be contaminated with RNA. A decision was made to continue using these PCR products to generate a 16S rDNA sequence of *S. "purple"*. Nucleic acid

concentration of the products were at the lower limit required for sequencing (3.5 ng μL^{-1} and 2.7 ng μL^{-1}, Table 3.2).

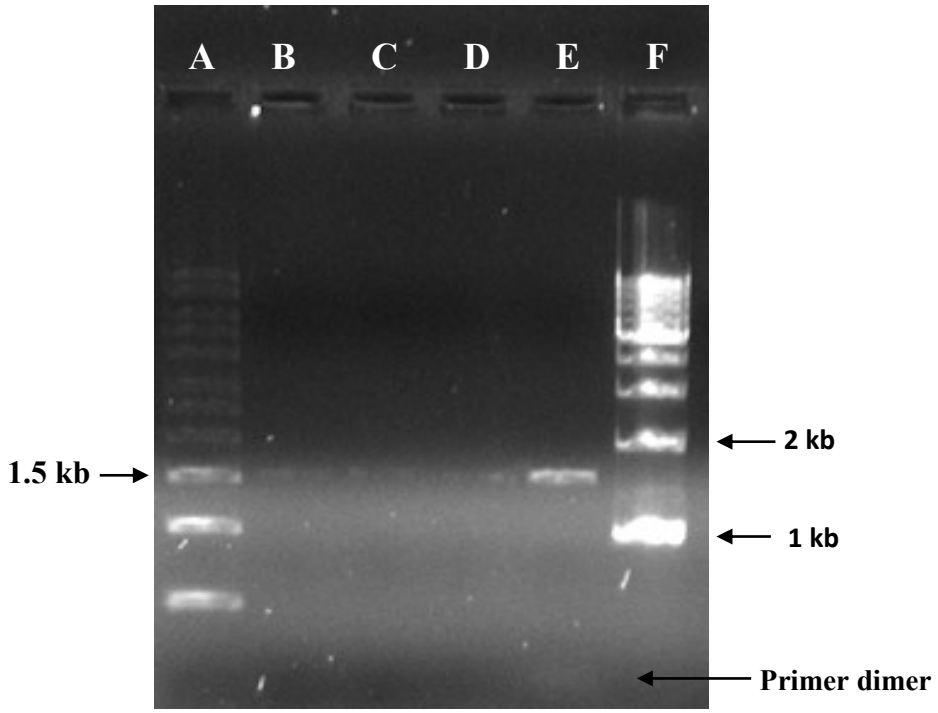

Figure 3.4: Purified PCR products gel. (Lane A) : Direct load 1kb DNA ladder (Sigma-Aldrich). (Lanes B and C) : Purified PCR products. (Lane D) : elution buffer. (Lane E) : unpurified PCR product. (Lane F) : 1kb step ladder (Promega).

Table 3.2: A260/280 values and concentration and of purified 16S rDNA PCR products from *S. "purple"*

S. "purple" 16S rDNA	Nucleic acid conc. (ng μL^{-1})	A260/280
Sample 1	3.5	2.35
Sample 2	2.7	2.13

3.1.4 Sequencing

Two template samples were submitted for sequencing using the forward and reverse primers, yielding four sequencing results. A 556 bp forward sequence and a 672 bp reverse sequence were obtained for one of the samples while a 430 bp forward sequence and a 844 bp reverse sequence were obtained for the other sample (Table 3.3, Appendix 1). The forward and reverse sequences of the first sample both had <100 (<20%) Q20 bases detected, while the forward and reverse sequences of the other sample had 408 (95%) and 683 (81%) Q20 bases detected respectively (Table 3.3).

Table 3.3: Raw sequence length and Q20 bases of *S. "purple"* rDNA sequences

Sample Tube	Raw Sequence length (bp)	Q20 bases (bp)	Q20 bases (%)
Purified 16S sample 1 + *16Sforwhole*	556	95	17
Purified 16S sample 1 + *16Srevwhole*	672	89	13
Purified 16S sample 2 + *16Sforwhole*	430	408	95
Purified 16S sample 2 + *16Srevwhole*	844	683	81

The sequences from sample 2 were determined to be more reliable than the sequences of sample 1 via their respective Q20 base scores and so were used in the assembly of a 1454 bp 16S rDNA sequence of *S. "purple"* (Appendix 6.2). The 1454 bp 16S rDNA sequence of *S. "purple"* was aligned with 115 other *Streptomyces* species, 2 *Kitasatospora* species and *M. tuberculosis* (Appendix 6.3) and a phylogenetic tree was constructed.

3.1.5 Phylogenetic analysis of 16S rDNA isolated from *S. "purple"*

The phylogenetic tree, including *S. "purple"*, 115 other *Streptomyces* species, 2 *Kitasatospora* species and *M. tuberculosis* (Fig. 3.5), placed *S. "purple"* in the *S. violaceoruber* clade with greater than 95% bootstrap support. This clade also includes several other species such as *S. violaceoruber*, *S. violaceolatus*, *S. humiferus*, *S. fragilis*, *S. coelicoflavus*, *S. anthocyanicus*, *S. tricolor and S. coelescens*.

The relationship between members of other established *Streptomyces* clades is also shown. *Streptomyces albidoflavus*, *S. coelicolor*, *S. champvatii* and *S. sampsoni* were grouped together in the *S. albidoflavus* clade with 99% bootstrap support. *Streptomyces griseus*, *S. microflavus*, *S. alboviridis*, *S. anulatus* and *S. acrimycini* were grouped together in the *S. griseus* clade with 99% bootstrap support.

The two members of the *Kitasatospora* genus, *K. atroaurantica* and *K. mediocidica*, were grouped together with 100% bootstrap support. *Kitasatospora* was nested

within *Streptomyces* with 96% bootstrap support indicating *Streptomyces* is paraphyletic.

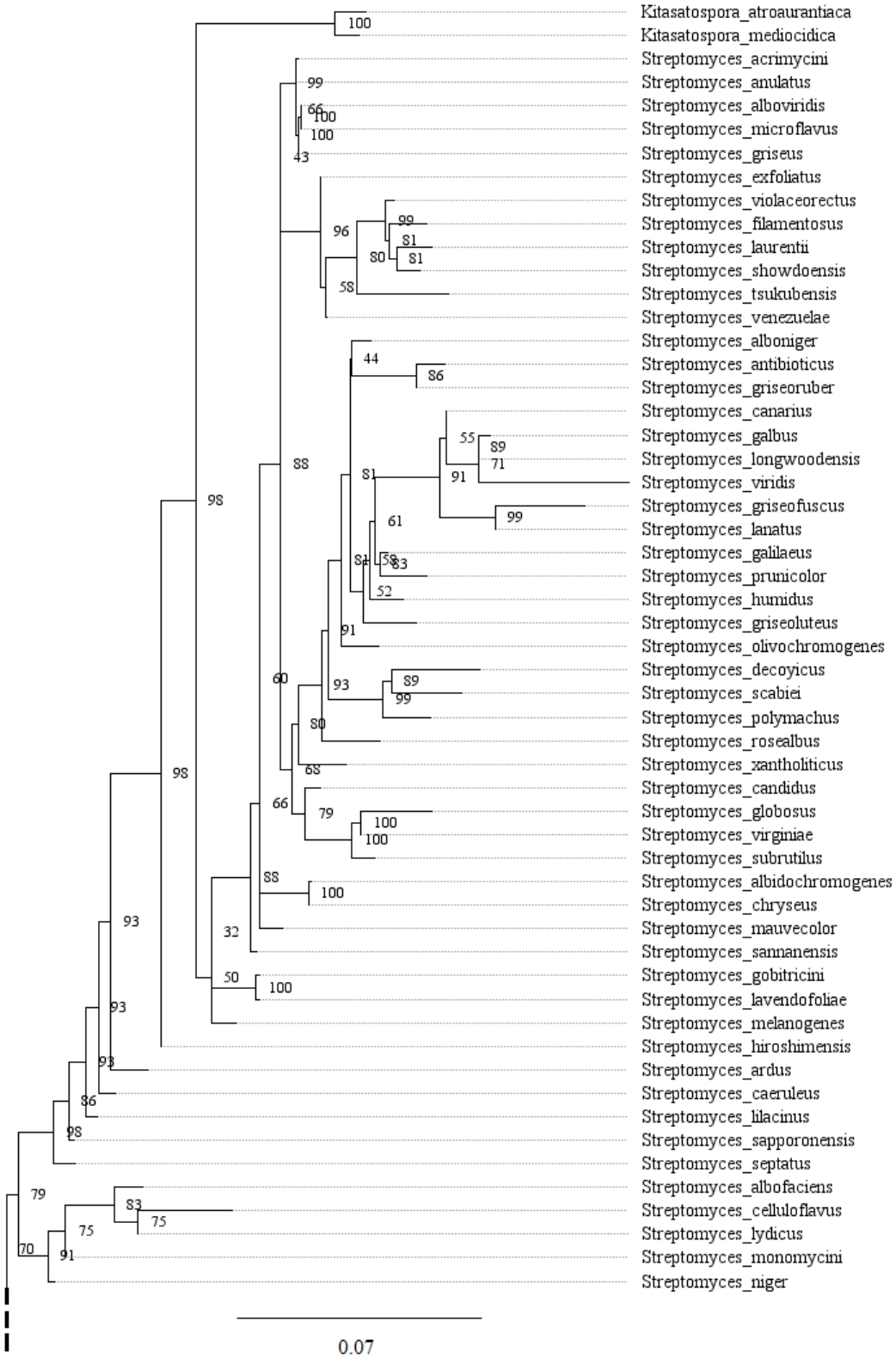

Figure 3.5 Phylogenetic tree (continued on following page) obtained by ML analysis based on 6S sequences. Values at nodes are bootstrap support approximations from the maximum likelihood analysis

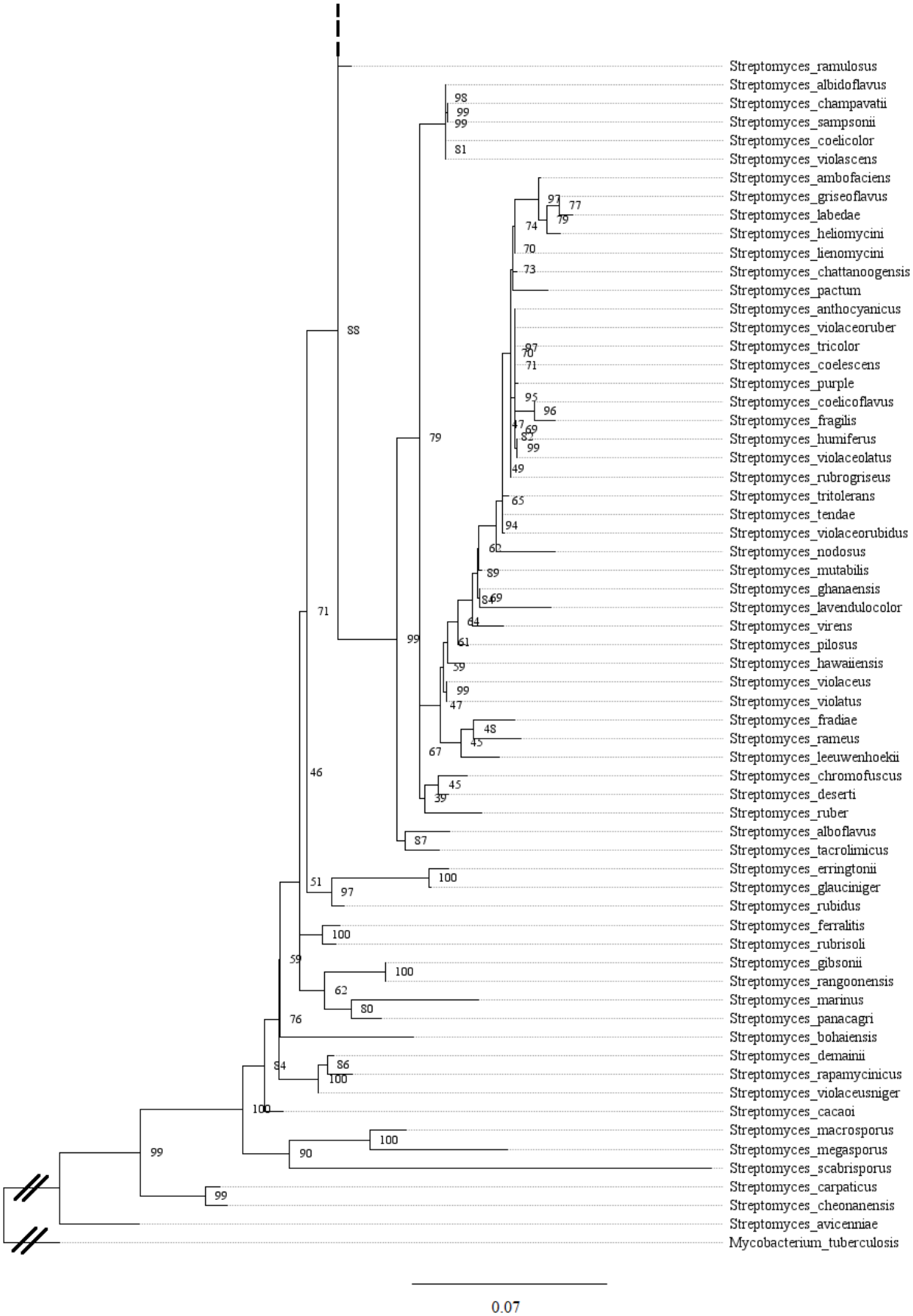
Streptomyces_ramulosus
Streptomyces_albidoflavus
Streptomyces_champavatii
Streptomyces_sampsonii
Streptomyces_coelicolor
Streptomyces_violascens
Streptomyces_ambofaciens
Streptomyces_griseoflavus
Streptomyces_labedae
Streptomyces_heliomycini
Streptomyces_lienomycini
Streptomyces_chattanoogensis
Streptomyces_pactum
Streptomyces_anthocyanicus
Streptomyces_violaceoruber
Streptomyces_tricolor
Streptomyces_coelescens
Streptomyces_purple
Streptomyces_coelicoflavus
Streptomyces_fragilis
Streptomyces_humiferus
Streptomyces_violaceolatus
Streptomyces_rubrogriseus
Streptomyces_tritolerans
Streptomyces_tendae
Streptomyces_violaceorubidus
Streptomyces_nodosus
Streptomyces_mutabilis
Streptomyces_ghanaensis
Streptomyces_lavendulocolor
Streptomyces_virens
Streptomyces_pilosus
Streptomyces_hawaiiensis
Streptomyces_violaceus
Streptomyces_violatus
Streptomyces_fradiae
Streptomyces_rameus
Streptomyces_leeuwenhoekii
Streptomyces_chromofuscus
Streptomyces_deserti
Streptomyces_ruber
Streptomyces_alboflavus
Streptomyces_tacrolimicus
Streptomyces_erringtonii
Streptomyces_glauciniger
Streptomyces_rubidus
Streptomyces_ferralitis
Streptomyces_rubrisoli
Streptomyces_gibsonii
Streptomyces_rangoonensis
Streptomyces_marinus
Streptomyces_panacagri
Streptomyces_bohaiensis
Streptomyces_demainii
Streptomyces_rapamycinicus
Streptomyces_violaceusniger
Streptomyces_cacaoi
Streptomyces_macrosporus
Streptomyces_megasporus
Streptomyces_scabrisporus
Streptomyces_carpaticus
Streptomyces_cheonanensis
Streptomyces_avicenniae
Mycobacterium_tuberculosis
0.07

3.2 Development of methods for imaging *S. "purple"* vesicles

Having determined that *S. "purple"* was a *Streptomyces* strain, the availability of a reliable source of droplets in the laboratory allowed for development of methods for EV image analyses. Imaging of *Streptomyces* vesicles in the literature has been performed using TEM, however these facilities were not readily available or easily accessible compared with STEM facilities. Methods were developed to image *Streptomyces* vesicles with STEM using droplets produced by *S. "purple"* as a source of vesicles.

STEM was successfully used to image extracellular vesicles in droplets produced by *S. "purple"* (Fig. 3.6) though optimisation was required. Images taken at 15 kV only showed black structures (Fig. 3.6A), indicating the electron beam was not penetrating the sample and reaching the TED detector. A higher contrast was observed when the electron beam voltage was increased to 25 kV, revealing a number of spherical structures with a dark centre and bright outside ring (Fig. 3.6B) that was consistent with other EVs imaged with STEM (Fig. 3.6C) (Burlaud-Gaillard et al 2014), and *Streptomyces* EVs imaged with TEM (Fig. 3.6D) (Schrempf & Merling 2015).

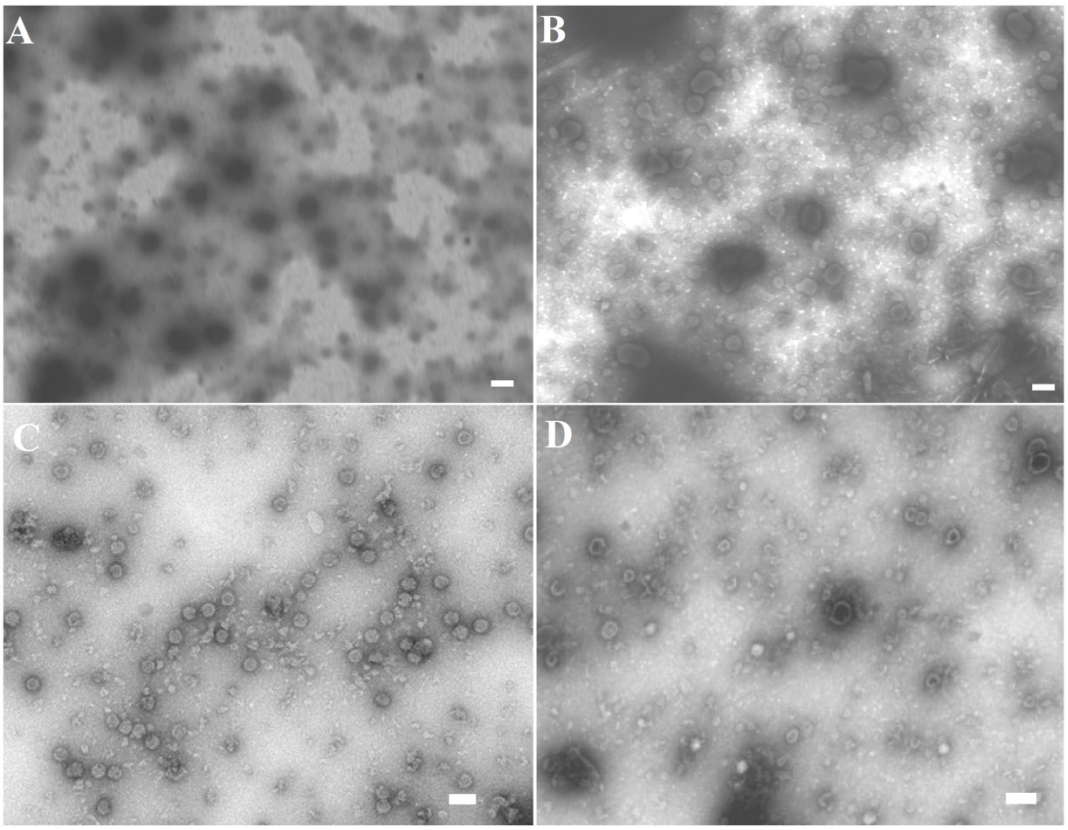

Figure 3.6 STEM images of droplet exudates produced by *S. "purple"*. **(**A): Numerous spherical dark structures of sizes ~60 - 120 nm observed at 15 kV. (B): Numerous spherical structures of sizes ~60 - 120 nm with internal contrast showing dark centres surrounded by a bright ring observed at 25 kV. (C): STEM image of EVs in literature (Burlaud-Gaillard et al 2014). (D) TEM image of *Streptomyces* EVs in literature (Schrempf & Merling 2015). Scale bars: 100 nm

3.3 Imaging of vesicles from *S. nodosus* strains

Following the development of methods for imaging *Streptomyces* EVs with STEM, experiments were undertaken to see if EVs were produced in liquid cultures from wildtype *S. nodosus* and *S. nodosus* MAΩ*hyg*, a mutant strain deficient in amphotericin B production. Biomass was crudely separated from culture fluid by size

fractionation and prepared on grids for analysis with STEM. As the *S. "purple"* STEM images showed more contrast with a higher electron beam voltage, STEM imaging of *S. nodosus* and *S. nodosus* MAΩ*hyg* culture fluid extracts was performed using the highest possible electron beam voltage (30 kV) offered by the JEOL-7001F SEM when operating in STEM mode.

EVs of various sizes were observed with STEM in both the *S. nodosus* (Fig. 3.7) and *S. nodosus* MAΩ*hyg* (Fig. 3.8) >100 kDa size fractionated samples, appearing as dark circles with a light ring near the edge. There was no significant size or morphology differences between the vesicles of *S. nodosus* (27-151 nm) and vesicles of *S. nodosus* MAΩ*hyg* (35-163 nm), with *S. nodosus* having a mean vesicle diameter and standard deviation of 84 ± 33 nm (n=22) and the mutant having an average vesicle diameter and standard deviation of 84 ± 33 nm (n=26) (Appendix 6.4). EVs were not detected in the <100 kDa fraction of *S. nodosus* culture broth (data not shown).

A >100 kDa fraction of *S. nodosus* culture broth was also analysed by TEM for comparison of image quality generated by STEM and EVs were observed (Fig. 3.9). The EVs observed with TEM were much brighter than *S. nodosus* EVs imaged with STEM (Fig. 3.7), however the TEM image had poorer resolution.

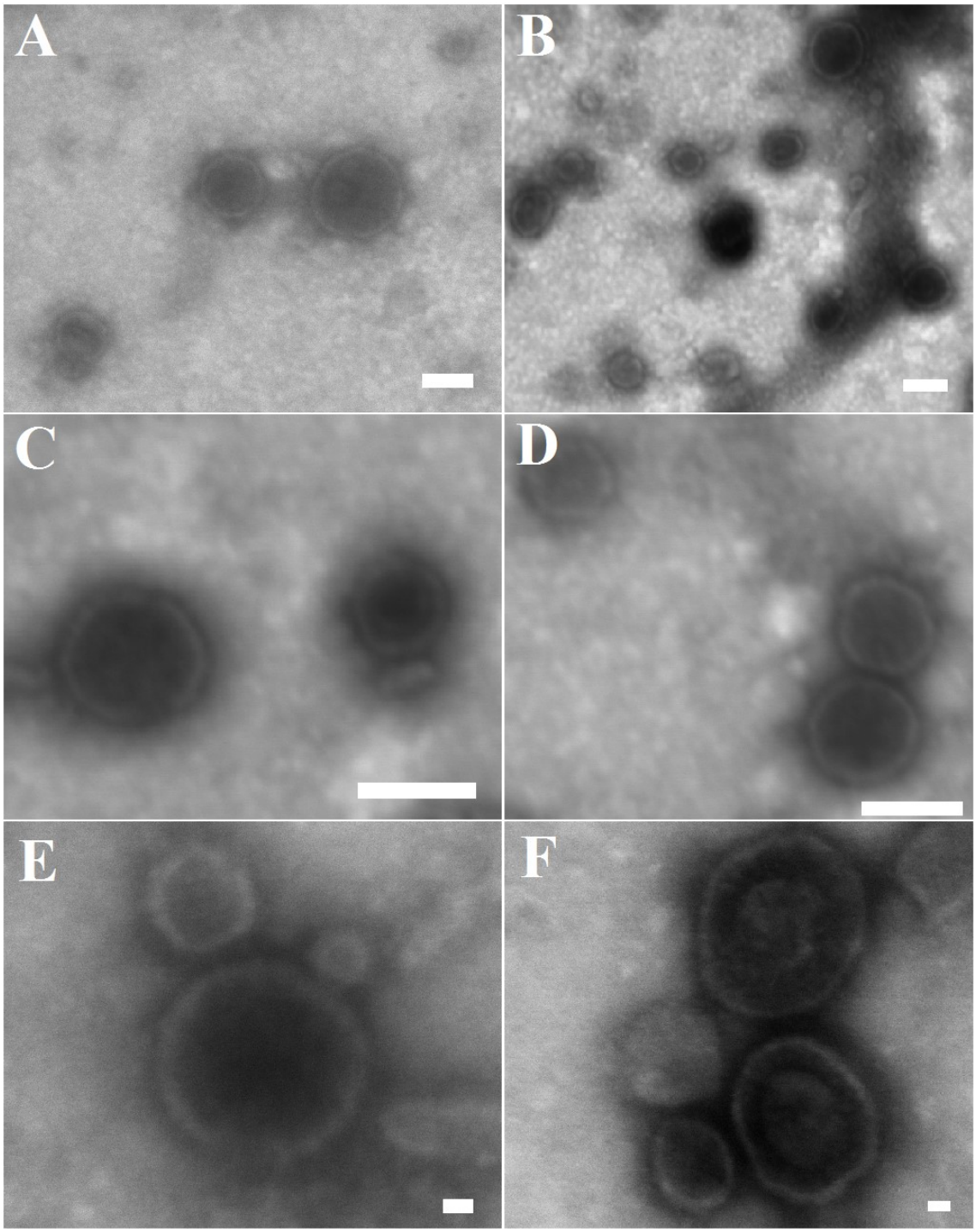

Figure 3.7: STEM analysis of a >100 kDa fraction of wildtype *S. nodosus* culture broth. (A - F): Numerous spherical EVs of various sizes (~30 - 150 nm). Scale bars: 100 nm in A - D; 10 nm in E and F.

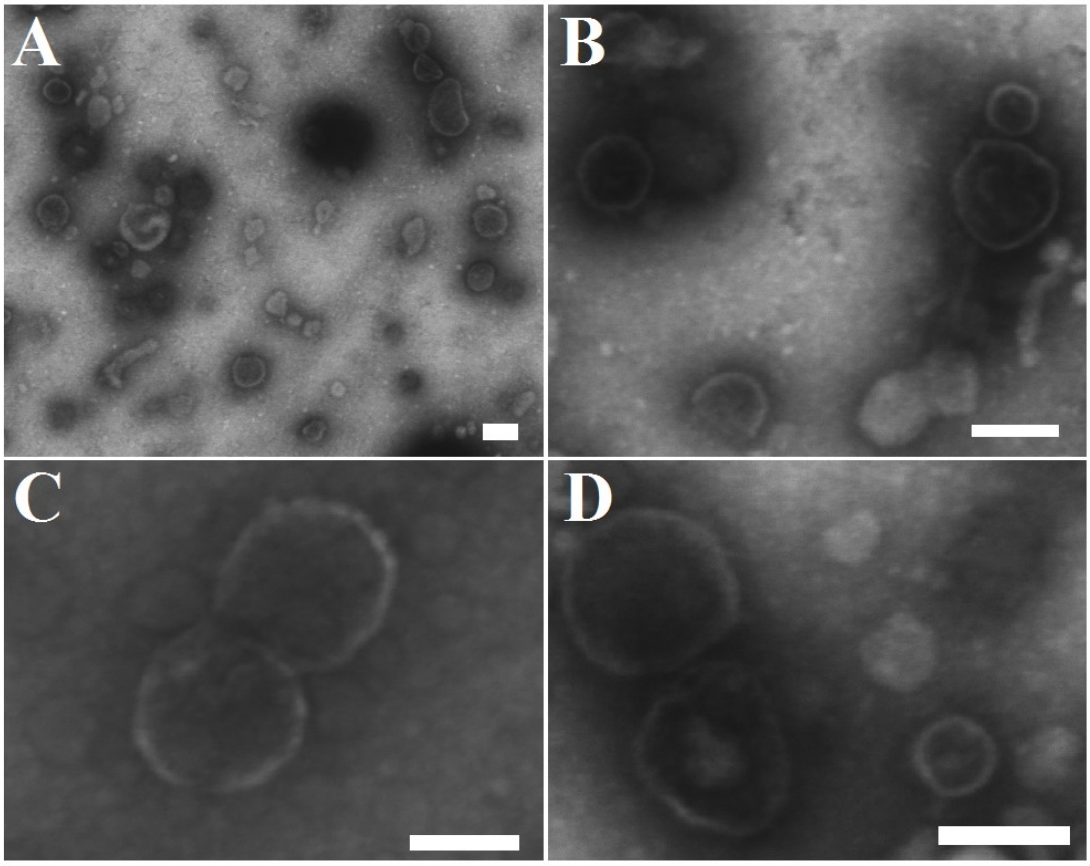

Figure 3.8: STEM analysis of a >100 kDa fraction of *S. nodosus* MAΩ*hyg* culture broth. (A-D): Numerous spherical EVs of various sizes (~30 - 160 nm). Scale bars: 100 nm.

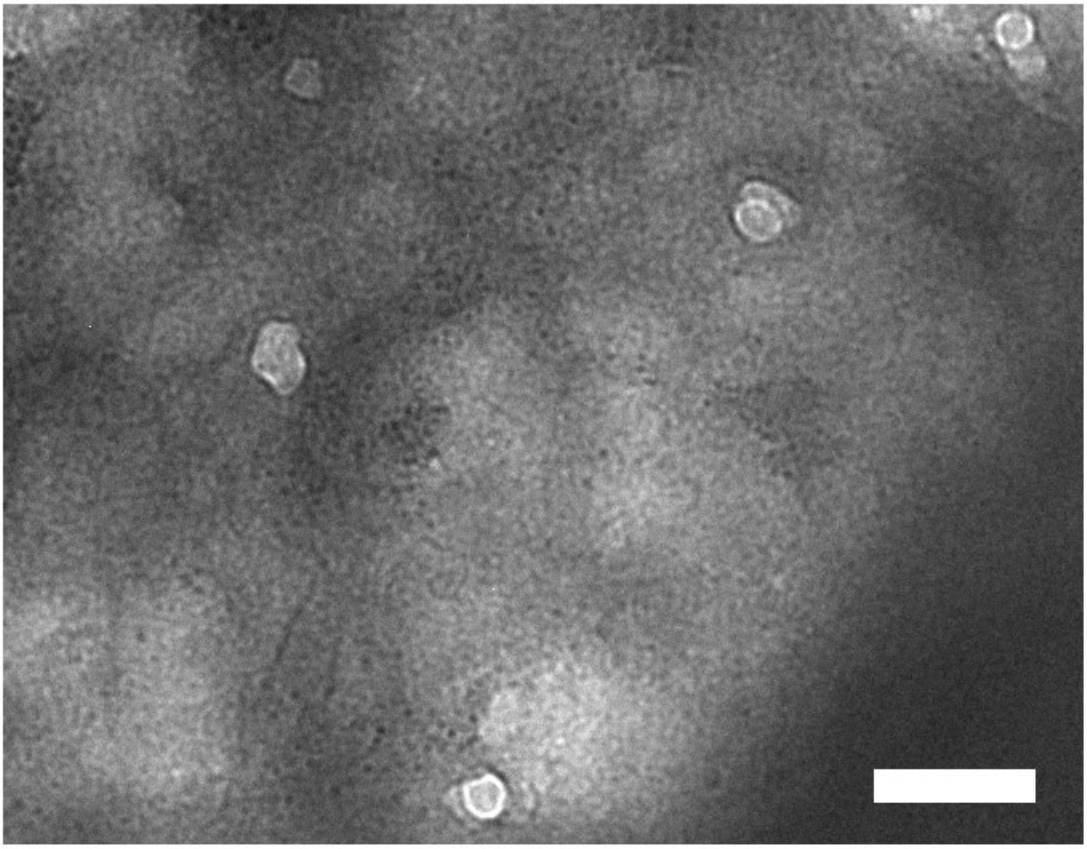

Figure 3.9: TEM analysis of a >100 kDa fraction of *S. nodosus* culture broth. Spherical EVs of sizes ~50 nm appearing as circles with a bright outside ring. Scale bar :200 nm.

3.4 Co-localisation of amphotericin B with EVs of *S. nodosus* strains

3.4.1 Confirming production of amphotericin B by the *S. nodosus* strains

UV-Vis spectroscopy was used to analyse samples extracted from the culture broth of *S. nodosus* and *S. nodosus* MAΩ*hyg* with DMSO and methanol to confirm production of amphotericin B by the wildtype *S. nodosus* strain. The UV-Vis spectra of the wildtype *S. nodosus* culture fluid extract (Fig. 3.10) showed strong peaks at

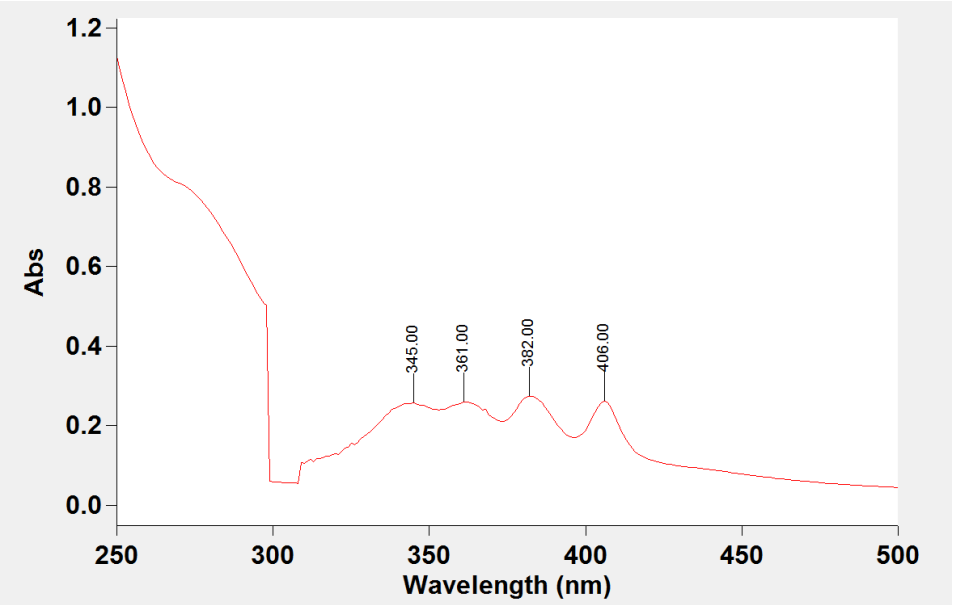

Figure 3.10 UV-Vis spectra (500-250 nm) of a culture broth extract from wildtype *S. nodosus*. Shifts were detected at 345 nm, 361 nm, 382 nm and 406 nm indicating the production of amphotericin B by the wildtype strain.

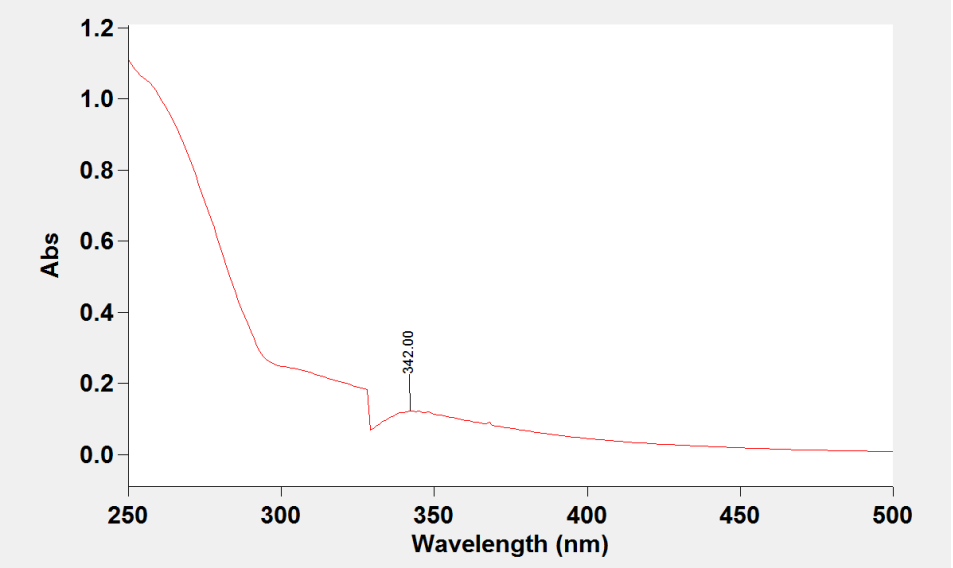

Figure 3.11 UV spectra (500-250 nm) of a culture broth extract from *S. nodosus* MAΩ*hyg*. No major peaks were observed indicating amphotericin B was not being produced by the mutant strain.

345 nm, 361 nm, 382nm and 406 nm which are consistent with amphotericin B (McNamara et al 1998) indicating the wildtype *S. nodosus* strain was producing amphotericin B.

In contrast the UV-Vis analysis of the *S. nodosus* MAΩ*hyg* extract (negative control, Fig. 3.11) showed the spectra had no major peaks which indicated the mutant was not producing amphotericin B.

3.4.2 Co-localisation of amphotericin B in size fractionated *S. nodosus* culture broth extracts

UV-Vis spectroscopy was also used to investigate whether EVs produced by *S. nodosus* and amphotericin B co-localised during size fractionation. As STEM investigations had shown a <100 kDa fraction of *S. nodosus* culture broth was free of EVs, it was hypothesised that the fraction would have a low concentration of amphotericin B if amphotericin B was associated with EVs. A cell free culture broth was passed through a 100 kDa molecular weight cut off filter device to obtain a <100 kDa filtrate. Equal volumes of the cell-free culture broth and the <100 kDa fraction were analysed for amphotericin B content using UV-Vis spectroscopy (500-250 nm).

The UV-Vis spectra of the cell free *S. nodosus* culture broth showed peaks at 343 nm, 368 nm, 382 nm and 406 nm (Fig. 3.12). These peaks are very similar to the predicted amphotericin B shifts at 346 nm, 364 nm, 382 nm and 405 nm (McNamara et al 1998). In contrast the spectra of the <100 kDa fraction had no major peaks,

although small peaks at 342 nm and 368nm were detected. The peak at 342 nm could be an artefact similar to the one seen for *S. nodosus* MAΩ*hyg* (Fig. 3.11). The small shift at 368 nm for the <100 kDa fraction (Fig. 3.12) was also observed in all other UV-Vis spectra (Fig. 3.10, 3.11) which indicated these shifts were noise. Furthermore, the existence of this noise indicated that the observed shift for *S. nodosus* culture broth (Fig. 3.11) at 368 nm could also be noise, giving rise to the possibility of a masked peak at 364 nm, as is characteristic of one of the four signals corresponding with amphotericin B.

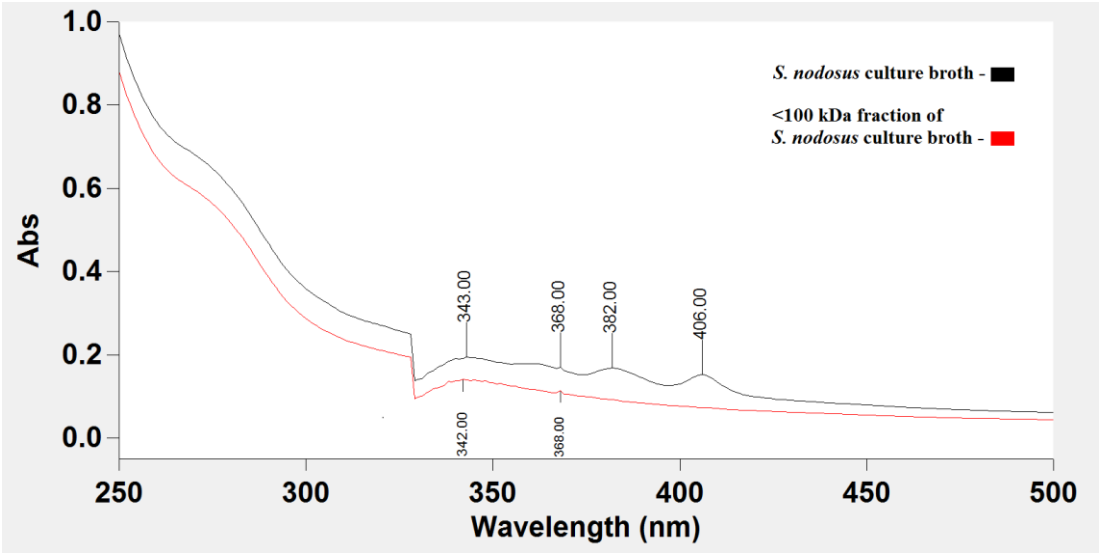

Figure 3.12: UV spectra (500-250 nm) of *S. nodosus* culture broth extracts. (Black) : *S. nodosus* culture broth extract showing peaks at 343 nm 368 nm 382 nm and 406 nm indicating the presence of amphotericin B. (Red) : A <100 kDa fraction of the *S. nodosus* culture broth extract showing no major peaks.

The UV-Vis spectra of these two samples (Fig. 3.12) indicated that the removal of vesicles and other >100 kDa content by size fractionation from *S. nodosus* culture

broth significantly reduced or eliminated amphotericin B concentration in the broth. This result suggests that *S. nodosus* co-localises amphotericin B in EVs.

CHAPTER 4

DISCUSSION

Drug delivery is an important area of pharmacological research because despite a drug having bioactivity, its administration in the human body can be problematic (Mitragotri et al 2014). As outlined previously, amphotericin B has been packaged into liposomes to circumvent toxicity issues (Adler-Moore 1994), some of which have been attributed to insolubility due to the drug's hydrophobicity (Liu et al 2017). This project investigated how *S. nodosus* addresses this issue. As the natural producer of this drug, the organism excretes the drug into an aqueous environment and must have developed mechanisms to do so. From studying this model, insight into how nature has evolved to solve this problem may provide information to be used in the pharmacology industry.

EVs are being explored as a mechanism for distribution of biomolecules into complex environments in nature and medicine (Brown et al 2015, Schwechheimer & Kuehn 2015). By using EV delivery systems hydrophobicity issues could be overcome, protection from chemical and biotic degradation could occur and targeted delivery of contents may be possible. All these issues are important aspects of drug delivery (Mitragotri et al 2014). Before analysing amphotericin B delivery via vesicles, methods needed to be developed and established in our laboratory.

4.1 Taxonomy of *S. "purple"* - a model organism for development of vesicle imaging techniques

Streptomyces "purple" had been shown to produce extracellular droplets on the surface of mycelia on repeated subculture, while other organisms in our laboratory lost this capacity (Chuck, unpublished data). As *Streptomyces* droplets have been

shown to be a novel source of vesicles (Schrempf et al 2011, Schrempf & Merling 2015) it was decided to use droplets produced by *S. "purple"* as a model to develop vesicle imaging techniques. At the beginning of the project there was limited evidence that the organism was a *Streptomyces* species, so concurrently with developing imaging methodology, taxonomic experiments were undertaken. To this end, gDNA was isolated from *S. "purple"* and PCR used to amplify the 16S rDNA sequence for phylogenetic analysis. The 16S rDNA sequence is highly conserved amongst bacteria and is widely used for taxonomic evaluation of these organisms (Srinivasan et al 2015).

The observed sizes (>10 kb) of *S. "purple"* gDNA by electrophoresis were consistent with sizes of gDNA isolated from other *Streptomyces* species using the same technique that were >30 kb (Nikodinovic et al 2003). While the gDNA isolation of *S. "purple"* and subsequent PCR reactions were successful, poor purification yield of the 16S rDNA products and high A260/280 ratios were observed, however sequenced data was still obtained. This may have caused the sequences to be shorter than expected. Fortunately the region containing the majority of missing nucleotides in the 1454 bp 16S rDNA sequence of *S. "purple"* is fairly well conserved amongst the other *Streptomyces* and *Kitasatospora* species used in the construction of the phylogenetic tree.

Through the construction of a phylogenetic tree based on 16S sequences it was determined that *S. "purple"* is a *Streptomyces* strain belonging to the *S. violaceoruber* clade. Interestingly the namesake and other members of the clade that *S. "purple"*

was placed into have the Latin prefix for violet, viola-, in their species names (Duangmal et al 2005) which is reminiscent of the purple pigment produced by *S. "purple"* when grown on GA agar. These results confirmed that the biological material of this strain was of *Streptomyces* origin.

The phylogenetic tree correctly grouped relationships within each of the *S. violaceoruber* (Duangmal et al 2005), *S. albidoflavus* (Rong et al 2009) and *S. griseus* clades (Rong & Huang 2010) with high bootstrap support values. Members of the *Kitasatospora* genus were nested within *Streptomyces*, which is consistent with a recent phylogenetic studies of *Kitasatospora* and *Streptomyces* species (Labeda et al 2012, Girard et al 2013, Girard et al 2014), indicating that *Streptomyces* is a paraphyletic genus.

The phylogenetic tree could have been improved by removing sequences from the analysis and changing the outgroup from *M. tuberculosis* to an organism more closely related to *Streptomyces*, like *Motilibacter peucedani*.

4.2 STEM imaging of vesicles in droplets produced by *S. "purple"*

To support work with EVs produced by *S. nodosus*, methods of imaging *Streptomyces* vesicles with STEM were first developed using droplets produced by *S. "purple"* as a model. EVs of sizes ~60 - 120 nm were observed in the *S. "purple"* droplet samples. These spherical structures shared the same morphology as *Streptomyces* EVs imaged with TEM, although they were somewhat smaller than *S. coelicolor* EVs that were 80 - 400 nm (Schrempf et al 2011) and *S. lividans* EVs

that were 20 - 230 nm (Schrempf & Merling 2015). After *S. coelicolor* and *S. lividans*, *S. "purple"* is the third *Streptomyces* species to have EV content in droplet exudates observed by electron microscopy, which supports the idea that delivery of biomolecules via this process is widespread amongst the genus. In addition, this is the first time STEM has been used to image *Streptomyces* EVs, although STEM has been used previously to image EVs of virus particles (Burlaud-Gailard et al 2014). Having a developed method for imaging *Streptomyces* EVs with STEM facilitated the imaging of EVs isolated from the culture broth of *S. nodosus* strains.

4.3 Imaging EVs isolated from culture broth extracts of *S. nodosus* strains

The existence of EVs in the culture broths of *S. nodosus* strains was confirmed using STEM. This is the first time EVs have been detected in *S. nodosus* culture broth. EVs were detected in the culture broth extracts of the knockout mutant *S. nodosus* MAΩ*hyg* that had the same morphology and size (84 ± 33 nm) as EVs of the wildtype. Production of vesicles by the mutant strain was expected as EVs are utilised by organisms in the three domains of life for a diverse range of processes beyond the delivery of polyketide drugs (Deatherage & Cookson 2012, Brown et al 2015, Schwechheimer & Kuehn 2015). This means that EVs are used by *S. nodosus* to deliver or protect important molecules other than amphotericin B.

EVs were not observed in a <100 kDa fraction of *S. nodosus* culture broth using STEM, showing that size fractionation is an effective technique to extract EVs from

culture fluid. This result supported the co-localisation experiments by confirming the <100 kDa size fractionated sample of *S. nodosus* culture broth was free of EVs.

To verify that the STEM images were of high quality, vesicles produced by wildtype *S. nodosus* were also imaged using TEM. The images of *S. nodosus* vesicles obtained in this study using STEM had better resolution than the images taken with TEM using identical sample preparation. Some of this may be attributed to having less operational experience using a TEM rather than TEM being an inferior technique to STEM. The TEM images did show a greater contrast of EVs with background material compared to EVs in the STEM images which is likely due to the TEM operating at 100 kV compared to 30 kV for STEM. These results show that for the imaging of *Streptomyces* EVs, STEM is an effective alternative to TEM.

Our sample preparation for STEM imaging of EVs could have been improved by gathering enough volume of droplet or vesicle samples so that TEM grids could be fully immersed inside drops (~100 µL) of the samples prior to fixation and staining.

4.4 Co-localisation of *S. nodosus* EVs with amphotericin B

The co-localisation of amphotericin B with EVs during size fractionation is the first evidence indicating that *S. nodosus* may use EVs to improve the solubility of amphotericin B in culture fluid. If this is correct then further characterisation may lead to improved therapeutic delivery systems of amphotericin B based on *S. nodosus* EVs, however more evidence is needed to conclude this definitively.

4.5 Future work

There are has several additional areas for further investigation as a result of this project, some of which could not be attempted due to time constraints. Further phylogenetic work could be undertaken to determine classification of *Kitasatospora* species and closely related *Streptomyces* species. The analysis could include the recently identified taxonomic marker SsgB. The amino acid sequences of SsgB proteins showed distinct differences between *Kitasatospora* and *Streptomyces* (Girard et al 2013, Girard et al 2014) and should be included in future phylogenetic reconstruction with a broader range of species.

Our UV-Vis analysis showed a qualitative relationship between *S. nodosus* EVs and amphotericin B concentration, however, quantifying this relationship with HPLC was the ultimate goal. To ascertain this relationship, vesicle isolation procedures need to be improved. Isolating EVs by size fractionation was sufficient for image analysis and preliminary co-localisation experiments, however, future studies need to be sure EVs are responsible for the effects we have seen. Purification of EVs using sucrose gradients (Klimentová & Stulík 2014) would allow further confidence that any amphotericin B detected via HPLC is associated with EVs and not other >100 kDa content. Once this is confirmed, chemical characterisation of the EVs could be undertaken.

One promising direction for this research is the loading of amphotericin B into EVs. Projects in our lab have shown that amphotericin B had improved solubility in the conditioned culture media of *S. nodosus* MAΩ*hyg* compared with YMG media

(Pereira 2007). In these experiments the media would have contained EVs from the amphotericin B deficient mutant which may have been responsible for the increased amphotericin B concentration. To investigate if these EVs package amphotericin B, they should first be isolated and purified through a sucrose gradient. Amphotericin B could be added to dilutions of purified EVs in DMSO until saturation and analysed with HPLC. Additional HPLC analysis could be performed on EVs loaded with amphotericin B using sonication, which can be used to package molecules into liposomes (Akbarzadeh et al 2013).

The association of amphotericin B with *S. nodosus* EVs and loaded *S. nodosus* MAΩ*hyg* EVs can be further demonstrated by confocal fluorescence microscopy. This technique has been used to show amphotericin B is associated with the membrane of giant unilamellar vesicles, liposomes that are ~10 μm in diameter (Grudzinkski et al 2016). Using this technique it should also be possible to show a similar phenomenon occurring within natural EVs, although the comparatively small size of *S. nodosus* EVs (~100 nm) may bring challenges.

4.6 Conclusion

There is a current need for improved treatments for systemic fungal mycoses. To solve this problem, EVs are being explored to improve antifungal drug delivery. Further characterisation of the mechanisms used by *S. nodosus* for hydrophobic drug delivery in nature may lead to insights important for the drug delivery of amphotericin B and treatment of serious fungal infections. Any knowledge gained could potentially be expanded to other hydrophobic drugs.

CHAPTER 5

REFERENCES

ADLER-MOORE, J. 1994. AmBisome targeting to fungal infections. *Bone Marrow Transplant,* 14 Suppl 5**,** S3-7.

AKBARZADEH, A., REZAEI-SADABADY, R., DAVARAN, S., JOO, S. W., ZARGHAMI, N., HANIFEHPOUR, Y., SAMIEI, M., KOUHI, M. & NEJATI-KOSHKI, K. 2013. Liposome: classification, preparation, and applications. *Nanoscale Res Lett,* 8**,** 102.

ANDERSON, T. M., CLAY, M. C., CIOFFI, A. G., DIAZ, K. A., HISAO, G. S., TUTTLE, M. D., NIEUWKOOP, A. J., COMELLAS, G., MARYUM, N., WANG, S., UNO, B. E., WILDEMAN, E. L., GONEN, T., RIENSTRA, C. M. & BURKE, M. D. 2014. Amphotericin forms an extramembranous and fungicidal sterol sponge. *Nat Chem Biol,* 10**,** 400-6.

BARTNER, E., ZINNES, H., MOE, R. A. & KULESZA, J. S. 1957. Studies on a new solubilized preparation of amphotericin B. *Antibiot Annu,* 5**,** 53-8.

BLESA, A. & BERENGUER, J. 2015. Contribution of vesicle-protected extracellular DNA to horizontal gene transfer in Thermus spp. *Int Microbiol,* 18**,** 177-87.

BROWN, L., WOLF, J. M., PRADOS-ROSALES, R. & CASADEVALL, A. 2015. Through the wall: extracellular vesicles in Gram-positive bacteria, mycobacteria and fungi. *Nat Rev Microbiol,* 13**,** 620-30.

BURLAUD-GAILLARD, J., SELLIN, C., GEORGEAULT, S., UZBEKOV, R., LEBOS, C., GUILLAUME, J. M. & ROINGEARD, P. 2014. Correlative scanning-transmission electron microscopy reveals that a chimeric flavivirus is released as individual particles in secretory vesicles. *PLoS One,* 9**,** e93573.

CAFFREY, P., LYNCH, S., FLOOD, E., FINNAN, S. & OLIYNYK, M. 2001. Amphotericin biosynthesis in Streptomyces nodosus: deductions from analysis of polyketide synthase and late genes. *Chem Biol,* 8**,** 713-23.

CHUCK, J. A., DUNN, C., FACULTAD, F. E., NAKAZONO, C., NIKODINOVIC, J. & BARROW, K. D. 2006. Amplification of DNA encoding entire type I polyketide synthase domains and linkers from streptomyces species. *Curr Microbiol,* 53**,** 89-94.

CHUTKAN, H., MACDONALD, I., MANNING, A. & KUEHN, M. J. 2013. Quantitative and qualitative preparations of bacterial outer membrane vesicles. *Methods Mol Biol,* 966**,** 259-72.

DAS, S. & HALUSHKA, M. K. 2015. Extracellular vesicle microRNA transfer in cardiovascular disease. *Cardiovasc Pathol,* 24**,** 199-206.

DEATHERAGE, B. L. & COOKSON, B. T. 2012. Membrane vesicle release in bacteria, eukaryotes, and archaea: a conserved yet underappreciated aspect of microbial life. *Infect Immun,* 80**,** 1948-57.

DUANGMAL, K., WARD, A. C. & GOODFELLOW, M. 2005. Selective isolation of members of the Streptomyces violaceoruber clade from soil. *FEMS Microbiol Lett,* 245**,** 321-7.

EVANS, A. G., DAVEY, H. M., COOKSON, A., CURRINN, H., COOKE-FOX, G., STANCZYK, P. J. & WHITWORTH, D. E. 2012. Predatory activity of Myxococcus xanthus outer-membrane vesicles and properties of their hydrolase cargo. *Microbiology,* 158**,** 2742-52.

GHODHBANE-GTARI, F., HEZBRI, K., KTARI, A., SBISSI, I., BEAUCHEMIN, N., GTARI, M. & TISA, L. S. 2014. Contrasted reactivity to oxygen tensions in Frankia sp. strain CcI3 throughout nitrogen fixation and assimilation. *Biomed Res Int,* 2014**,** 568549.

GIRARD, G., TRAAG, B. A., SANGAL, V., MASCINI, N., HOSKISSON, P. A., GOODFELLOW, M. & VAN WEZEL, G. P. 2013. A novel taxonomic marker that discriminates between morphologically complex actinomycetes. *Open Biol,* 3**,** 130073.

GIRARD, G., WILLEMSE, J., ZHU, H., CLAESSEN, D., BUKARASAM, K., GOODFELLOW, M. & VAN WEZEL, G. P. 2014. Analysis of novel kitasatosporae reveals significant evolutionary changes in conserved developmental genes between Kitasatospora and Streptomyces. *Antonie Van Leeuwenhoek,* 106**,** 365-80.

GRUDZINSKI, W., SAGAN, J., WELC, R., LUCHOWSKI, R. & GRUSZECKI, W. I. 2016. Molecular organization, localization and orientation of antifungal antibiotic amphotericin B in a single lipid bilayer. *Sci Rep,* 6**,** 32780.

HAVLICKOVA, B., CZAIKA, V. A. & FRIEDRICH, M. 2008. Epidemiological trends in skin mycoses worldwide. *Mycoses,* 51 Suppl 4**,** 2-15.

KAMINSKI, D. M. 2014. Recent progress in the study of the interactions of amphotericin B with cholesterol and ergosterol in lipid environments. *Eur Biophys J,* 43**,** 453-67.

KAWABATA, M., ONDA, M. & MITA, T. 2001. Effect of aggregation of amphotericin B on lysophosphatidylcholine micelles as related to its complex formation with cholesterol or ergosterol. *J Biochem,* 129**,** 725-32.

KULLBERG, B. J. & ARENDRUP, M. C. 2015. Invasive Candidiasis. *N Engl J Med,* 373**,** 1445-56.

LABEDA, D. P., GOODFELLOW, M., BROWN, R., WARD, A. C., LANOOT, B., VANNCANNEYT, M., SWINGS, J., KIM, S. B., LIU, Z., CHUN, J., TAMURA, T., OGUCHI, A., KIKUCHI, T., KIKUCHI, H., NISHII, T., TSUJI, K., YAMAGUCHI, Y., TASE, A., TAKAHASHI, M., SAKANE, T., SUZUKI, K. I. & HATANO, K. 2012. Phylogenetic study of the species within the family Streptomycetaceae. *Antonie Van Leeuwenhoek,* 101**,** 73-104.

LIU, M., CHEN, M. & YANG, Z. 2017. Design of amphotericin B oral formulation for antifungal therapy. *Drug Deliv,* 24**,** 1-9.

MASHBURN, L. M. & WHITELEY, M. 2005. Membrane vesicles traffic signals and facilitate group activities in a prokaryote. *Nature,* 437**,** 422-5.

McNAMARA, C., BOX, S., CRAWFORTH, J. M., HICKMAN, B. S., NORWOOD, T. J. & RAWLINGS, B. J. 1998. Biosynthesis of amphotericin B. *J Chem Soc Perkin Trans,* 1**,** 83-87.

MIELANCZYK, L., MATYSIAK, N., KLYMENKO, O. & WOJNICZ, R. 2015. Transmission Electron Microscopy of Biological Samples, The Transmission Electron Microscope - Theory and Applications, Dr KHAN MAAZ (Ed), InTech, DOI:10.5772/60680 Available from: https://www.intechopen.com/books/howtoreference/the-transmission-electron-microscope-theory-and-applications/transmission-electron-microscopy-of-biological-samples

MINH, B. Q., NGUYEN, M. A. & VON HAESELER, A. 2013. Ultrafast approximation for phylogenetic bootstrap. *Mol Biol Evol,* 30**,** 1188-95.

MITRAGOTRI, S., BURKE, P. A. & LANGER, R. 2014. Overcoming the challenges in administering biopharmaceuticals: formulation and delivery strategies. *Nat Rev Drug Discov,* 13**,** 655-72.

MOURI, R., KONOKI, K., MATSUMORI, N., OISHI, T. & MURATA, M. 2008. Complex formation of amphotericin B in sterol-containing membranes as evidenced by surface plasmon resonance. *Biochemistry,* 47**,** 7807-15.

NAWAZ, M., CAMUSSI, G., VALADI, H., NAZARENKO, I., EKSTROM, K., WANG, X., PRINCIPE, S., SHAH, N., ASHRAF, N. M., FATIMA, F., NEDER, L. & KISLINGER, T. 2014. The emerging role of extracellular vesicles as biomarkers for urogenital cancers. *Nat Rev Urol,* 11**,** 688-701.

NGUYEN, L. T., SCHMIDT, H. A., VON HAESELER, A. & MINH, B. Q. 2015. IQ-TREE: a fast and effective stochastic algorithm for estimating maximum-likelihood phylogenies. *Mol Biol Evol,* 32**,** 268-74.

NIKODINOVIC, J. 2004. 'Molecular geneteic of amphotericin biosynthesis in *Streptomyces nodosus*', PhD thesis, UNSW, Sydney NSW

NIKODINOVIC, J., BARROW, K. D. & CHUCK, J. A. 2003. High yield preparation of genomic DNA from Streptomyces. *Biotechniques,* 35**,** 932-4, 936.

PEREIRA, T. 2007. 'Cellular differentiation and antibiotic production by *Streptomyces nodosus* immobilised in alginate capsules', PhD thesis, UWS, Sydney NSW.

PEREIRA, T., NIKODINOVIC, J., NAKAZONO, C., DENNIS, G. R., BARROW, K. D. & CHUCK, J. A. 2008. Community structure and antibiotic production of Streptomyces nodosus bioreactors cultured in liquid environments. *Microb Biotechnol,* 1**,** 373-81.

PERNODET, J. L., BOCCARD, F., ALEGRE, M. T., GAGNAT, J. & GUERINEAU, M. 1989. Organization and nucleotide sequence analysis of a ribosomal RNA gene cluster from Streptomyces ambofaciens. *Gene,* 79**,** 33-46.

PRANGISHVILI, D., HOLZ, I., STIEGER, E., NICKELL, S., KRISTJANSSON, J. K. & ZILLIG, W. 2000. Sulfolobicins, specific proteinaceous toxins produced by strains of the extremely thermophilic archaeal genus Sulfolobus. *J Bacteriol,* 182**,** 2985-8.

RICHARDSON, M. D. 2005. Changing patterns and trends in systemic fungal infections. *J Antimicrob Chemother,* 56 Suppl 1**,** i5-i11.

ROEMER, T. & KRYSAN, D. J. 2014. Antifungal drug development: challenges, unmet clinical needs, and new approaches. *Cold Spring Harb Perspect Med,* 4.

RONG, X., GUO, Y. & HUANG, Y. 2009. Proposal to reclassify the Streptomyces albidoflavus clade on the basis of multilocus sequence analysis and DNA-DNA hybridization, and taxonomic elucidation of Streptomyces griseus subsp. solvifaciens. *Syst Appl Microbiol,* 32**,** 314-22.

RONG, X. & HUANG, Y. 2010. Taxonomic evaluation of the Streptomyces griseus clade using multilocus sequence analysis and DNA-DNA hybridization, with proposal to combine 29 species and three subspecies as 11 genomic species. *Int J Syst Evol Microbiol,* 60**,** 696-703.

S, E. L. A., MAGER, I., BREAKEFIELD, X. O. & WOOD, M. J. 2013. Extracellular vesicles: biology and emerging therapeutic opportunities. *Nat Rev Drug Discov,* 12**,** 347-57.

SCHREMPF, H., KOEBSCH, I., WALTER, S., ENGELHARDT, H. & MESCHKE, H. 2011. Extracellular Streptomyces vesicles: amphorae for survival and defence. *Microb Biotechnol,* 4**,** 286-99.

SCHREMPF, H. & MERLING, P. 2015. Extracellular Streptomyces lividans vesicles: composition, biogenesis and antimicrobial activity. *Microb Biotechnol,* 8**,** 644-58.

SCHWECHHEIMER, C. & KUEHN, M. J. 2015. Outer-membrane vesicles from Gram-negative bacteria: biogenesis and functions. *Nat Rev Microbiol,* 13**,** 605-19.

SHIRLING, E. B. & GOTTLIEB D. 1966. Methods for characterization of Streptomyces species. *Int J Syst Evol Microbiol,* 16**,** 313-340.

SINGH, G., KAUR, T., KAUR, A., KAUR, R. & KAUR, R. 2014. Analytical methods for determination of Amphotericin B in biological samples: a short review. *AABS,* 1**,** R26-32.

SOUZA, A. C. & AMARAL, A. C. 2017. Antifungal Therapy for Systemic Mycosis and the Nanobiotechnology Era: Improving Efficacy, Biodistribution and Toxicity. *Front Microbiol,* 8**,** 336.

SRINIVASAN, R., KARAOZ, U., VOLEGOVA, M., MACKICHAN, J., KATO-MAEDA, M., MILLER, S., NADARAJAN, R., BRODIE, E. L. & LYNCH, S. V. 2015. Use of 16S rRNA gene for identification of a broad range of clinically relevant bacterial pathogens. *PLoS One,* 10**,** e0117617.

TACCONE, F. S., VAN DEN ABEELE, A. M., BULPA, P., MISSET, B., MEERSSEMAN, W., CARDOSO, T., PAIVA, J. A., BLASCO-NAVALPOTRO, M., DE LAERE, E., DIMOPOULOS, G., RELLO, J., VOGELAERS, D., BLOT, S. I. & ASP, I. C. U. S. I. 2015. Epidemiology of invasive aspergillosis in critically ill patients: clinical presentation, underlying conditions, and outcomes. *Crit Care,* 19**,** 7.

TASHIRO, Y., ICHIKAWA, S., NAKAJIMA-KAMBE, T., UCHIYAMA, H. & NOMURA, N. 2010. Pseudomonas quinolone signal affects membrane vesicle production in not only gram-negative but also gram-positive bacteria. *Microbes Environ,* 25**,** 120-5.

VAN DER MEEL, R., FENS, M. H., VADER, P., VAN SOLINGE, W. W., ENIOLA-ADEFESO, O. & SCHIFFELERS, R. M. 2014. Extracellular vesicles as drug delivery systems: lessons from the liposome field. *J Control Release,* 195**,** 72-85.

WILCOCK, B. C., ENDO, M. M., UNO, B. E. & BURKE, M. D. 2013. C2'-OH of amphotericin B plays an important role in binding the primary sterol of human cells but not yeast cells. *J Am Chem Soc,* 135**,** 8488-91.

APPENDIX 1

Forward 16S rDNA sequence of *S. "purple"* sample 1

```
1         10         20         30         40         50
|         |          |          |          |          |
AAAAGCGTTACGACTTCGCTAAGCTCGCCGCTTGCATAACATTGCACGTC
GAACGATGAATTTTTCGGTGGTGATTACTGGCCAACGTGTGATTAACACA
TTACCCAATCTGCCCTTCACTCTGGGACAAGCCTTGAAAACAGGGTCTAA
TACCGGATACTGACCCCCGCAAGCATCTGCGAGGTTCGAAAGCTCCGGCG
GCGTTTGATGACTTCGCGGCCTATCCCCTTGTTGGTGAGGTAACGGCTCA
CCCCTGCGACAAAAGTTACCCTGCCTGCCAGGGCGACCGGCCACTATGTG
ACTGAGACCCGCCCCCGACTCCTAATTTAGGCAGCATTGATAACCCCCCC
CTTGGGGCCAAATCCTGATGCCCCCACGCCGCGAGAAGGACGACCGCTTT
TGGGTTGTATACCTCTTGCGGCAGGGCGAATTTTTTCCGGTTTTTCCCTG
ATGAATGCCCGCTGCTATCTCTGTGGCCGCCTCAACGAAGATTCTTATGT
TGCACTTTTTGCACGGAAACCACCCCCACCAAAAACACTTTTGTTTCCCT
CGTCCT
```

Reverse 16S rDNA sequence of *S. "purple"* sample 1

```
1         10         20         30         40         50
|         |          |          |          |          |
GGCGAAAATACTCTCTTGGCAGCAGCTTCTCTTCCGTCATGGGACCGTGC
GACATGCCTATTCATACGAAACTCGGCCCATGGAACATGCTATGCTCGGT
TTTGCCCTGGGTATTCTCAAAAAGAAGTTCTCCTAAAAAAAACCGCCGCC
CAGGTTTAGACGCCAATCTAGTGCACCCTACCAAAACACGCCGATTCGGT
TATGTATGTTTAGGATCGTACGTCGTAGTGAGCAGTACCCTCCACCGCCT
TGAATATAAGTAACACTGCCATCTATGCAAAGTCCTAAATAATATTCCAC
ACTGCTCATTCGTAATTGTACGAGGAATGAATTATGACTCCGGCCTCTAA
CCCGAAGAACCCACCGGATGAACGGACCTGAAGACGACGAACAAGAAATT
CATCCCTCTAGTGGAGACTCGGGGTATTGATAGGGTTACTAAATTGAACG
CGAAATCGCTATCTCTGTTATCGCCGGAATAACGTTTCTTTTGTTACAAA
TAGGCTTTGGTATCCGCCTCCACGACAAACCCCATTTCTTTGCCGGTGAA
CGCCAAGTAGACGAAGGAATGACCCGTATCCACGCCAAGCCGGTACATGT
AGATACAAAGAAAACTGTGAATTTGATTCGCTGAAGGTCCACCTTTTCAC
GCTATTAGTGGAGGCATCCGTG
```

Forward 16S rDNA sequence of *S. "purple"* sample 2

```
1         10         20         30         40         50
|         |          |          |          |          |
TCGAACGATGAACCACTTCGGTGGGGATTAGTGGCGAACGGGTGAGTAAC
ACGTGGGCAATCTGCCCTTCACTCTGGGACAAGCCCTGGAAACGGGGTCT
AATACCGGATACTGACCCTCGCAGGCATCTGCGAGTTTCGAAAGCTCCGG
CGGTGAAGGATGAGCCCGCGGCCTATCATCTTGTTGGTGAGGTAATGGCT
CACCAAGGCGACGACGGGTAGCCGGCCTGAGAGGGCGACCGGCCACACTG
GGACTGAGACACGGCCCAGACTCCTACGGGAGGCAGCAGTGGGGAATATT
GCACAATGGGCGAAAGCCTGATGCAGCGACGCCGCGTGAGGGATGACGGC
CTTCGGGTTGTAAACCTCTTTCAGCATGGAAGAATCGAAAGTGACCTGTA
CCTGCCGAACAAGCGCCGGCTAACTACGTG
```

Reverse 16S rDNA sequence of *S. "purple"* sample 2

```
1         10         20         30         40         50
|         |          |          |          |          |
TTCGTCCCAATCGCCAGTCCCACCTTCGACAGCTCCCTCCCACAAGGGGT
TGGGCCACCGGCTTCGGGTGTTACCGACTTTCGTGACGTGACGGGCGGTG
TGTACAAGGCCCGGGAACGTATTCACCGCAGCAATGCTGATCTGCGATTA
CTAGCGACTCCGACTTCATGGGGTCGAGTTGCATACCCCAATCCGAACTG
AGACCGGCTTTTTGAGATTCGCTCCACCTTGCGGTATCGCAGCTCATTGT
ACCGGCCATTGTACCACGTGTGCATCCCAAGACATAAGGGGCATGATGAC
TTGACGTCCTCCCCACCTTCCTCCGAGTTGACCCCGGCGGTCTCCCGTGA
GTCCCCAACACCCCGAAGGGCTTGCTGGCAACACGGGACAAGGGTTGCGC
TCGTTGCGGGACTTAACCCAACATCTCACGACACGAGCTGACGACAGCCA
TGCACCACCTGTACACCGACCACAAGGGGGGCACCATCTCTGATGCTTTC
CGGTGTATGTCAAGCCTTGGTAAGGTTCTTCGCGTTGCGTCGAATTAACC
CACATGCTCCGCCGCTTGTGCGGGCCCCCGTCAATTCCTTTGAGTTTTAG
CCTTGCGGCCGTACTCCCCAGGCGGGGCACTTAATGCGTTAGCTGCGGCA
CGGACAACGTGGAAATGTTGCCCCACACCTAGTGCCCACCGTTTAGGCGT
GCACTACCAGGGTATCTAATCCTGTTCGCTCCCCACGCTTTCTCTCCTCA
GCGTCAGTATCGGCCCCAGAGATCCGTCTTCGCCACCGGTAGTCCCTCCT
GATATCTGCGCATTTCACCGCTACACCAGGAAATTCAGATCTCC
```

APPENDIX 2

1454 bp 16S rDNA sequence of *S. "purple"*

```
1        10        20        30        40        50
|        |         |         |         |         |
NNNNTCGAACGATGAACCACTTCGGTGGGGATTAGTGGCGAACGGGTGAG
TAACACGTGGGCAATCTGCCCTTCACTCTGGGACAAGCCCTGGAAACGGG
GTCTAATACCGGATACTGACCCTCGCANGCATCTGCGAGNNNNGAAAGCT
CCNGCGGTGAAGGATGAGCCCGCGGCCTATCNNCTTGTTGGTGAGGTAAT
GGCTCACCNNGGCGACNACGGGTAGCCGGCCNGANAGGGCGACCGGCCNC
ANTGGNACTGANACACGGCCCAGACTCCTANGGGAGGNAGCNNTGGGGAA
TATTGNNCAATGGGCGAAAGCCNGATGCAGCGACGCCGCGTGAGGGATGA
CGGCCTTCNGGTTGTAAACCTCTTTCNNCANGNAANNNNNNNNNNNNNNN
NNNNNNNNNNNNNNNNNNNNNNNNNNNNNNNNNNNNNNNNNNNNNNNNNN
NNNNNNNNNNNNNNNNNNNNNNNNNNNNNNNNNNNNNNNNNNNNNNNNNN
NNNNNNNNNNNNNNNNNNNNNNNNNNNNNNNNNNNNNNNNNNNNNNNNNN
NNNNNNNNNNNNNNNNNNNNNNNNNNNNNNNNNNNNNNNNNNNNNNNNNN
NNNNNNNNNNNNNNNNNNNNNNNNNNNNNNNNNNNNNNNNNNNNNNNNNN
NNNNNNNNNNNNNNNNNNNNNNNNNNNNNNNNNNNNNNNNNNNNNNNNNN
NNNNNNNNNNNNNNNNNNNNNNNNNNNNNNNNNNNNNNNNNNNNNNNNNN
NNNNNNNNNNNNNNNNNNNNNNNNNNNNNNNNNNNNNNNNNNNNNNNNNN
NNNNNNNNNNNNNNNNNNNNNNNNNNNNNNNNNNNNNNNNNNNNNNNNNN
NNNNNNNNNNNNNNNNNNNNNNNNNNNNNNNNNTTAATTCGACGCAANGC
GAAGAACCTTACCAAGGCTTGACATACNCNNGAAAGCATCAGAGATGGTG
CCCCCNTNGTGGNNGGNGTACAGGTGGNGCANGGCTGTCGTCAGNTCGTG
TCGTGAGATGTTGGGTTAAGTCCNGCAACGAGCGNAACCCTTGTNNNNTG
TTGNCAGCAAGCCNTTNGGGGTGTTGGGGACTCACGGGAGACCGCCGGGG
TCAANTCGGAGGAAGGTGGGGANGANGTCAAGTCATCANGCCCNTTATGT
NTTGGGNTGCACACGTGNTNCAATGGCCGGTACAATGAGNTGNGATACCG
CAAGGTGGAGNGAATCTCAAAAAGCNGGTCTCAGTTNGGATNGGGGTNTG
CAACTCGACCCCATGAAGTCGGAGTCGNTAGTNNNNGCAGATCAGCATTG
NTGCGGNGAATACGTTCCCGGGCCTTGTACACACNGCCNGTCACGTCNNG
AAAGTNGGTAACACCNGAAGCCGGTGGCCCAACCCCNNGTGGGAGGGAGC
TGTT
```

APPENDIX 3

Table: A3.1 Sequence accession table for 16S rDNA sequences used for phylogenetic analysis

Organism	Accession number
Kitasatospora atroaurantiaca	DQ026645.1
Kitasatospora mediocidica	U93324.1
Mycobacterium tuberculosis	AM283534
Streptomyces acrimycini	AY999889.1
Streptomyces albidochromogenes	AB249953.1
Streptomyces albidoflavus	AB184255.1
Streptomyces albofaciens	AB045880.1
Streptomyces alboflavus	EF178699.1
Streptomyces alboniger	AY845349.1
Streptomyces alboviridis	AB184256.1
Streptomyces ambofaciens	AB184182.1
Streptomyces anthocyanicus	AB184631.1
Streptomyces antibioticus	AY999776.1
Streptomyces anulatus	DQ026637.1
Streptomyces ardus	AB184864.1
Streptomyces avicenniae	EU399234.1
Streptomyces bohaiensis	KF682221.2
Streptomyces cacaoi	AB184183.1
Streptomyces caeruleus	EF178675.1
Streptomyces canarius	AB184396.1
Streptomyces candidus	DQ026663.1
Streptomyces carpaticus	DQ442494.1
Streptomyces celluloflavus	AB184476.2
Streptomyces champavatii	DQ026642.1
Streptomyces chattanoogensis	AY295791.1
Streptomyces cheonanensis	AY822606.1
Streptomyces chromofuscus	AB184194.1
Streptomyces chryseus	AY999787.1
Streptomyces coelescens	AF503496.1
Streptomyces coelicoflavus	AB184650.1
Streptomyces coelicolor	AB184196.1
Streptomyces decoyicus	EU170127.1
Streptomyces demainii	DQ334782.1
Streptomyces deserti	HE577172.1
Streptomyces erringtonii	HE573871.1
Streptomyces exfoliatus	AB184324.1
Streptomyces ferralitis	AY262826.1
Streptomyces filamentosus	AB184130.1
Streptomyces fradiae	DQ026630.1
Streptomyces fragilis	AY999917.1

Organism	**Accession number**
Streptomyces galbus	X79852.1
Streptomyces galilaeus	AB045878.1
Streptomyces ghanaensis	AY999851.1
Streptomyces gibsonii	AB184663.1
Streptomyces glaucinger	AB249964.1
Streptomyces globosus	AJ781330.1
Streptomyces gobitricini	AB184666.1
Streptomyces griseoflavus	AJ781322.1
Streptomyces griseofuscus	AB184206.1
Streptomyces griseoluteus	AY999751.1
Streptomyces griseoruber	AB184209.1
Streptomyces griseus	AY207604.1
Streptomyces hawaiiensis	AB184143.1
Streptomyces heliomycini	AB184712.1
Streptomyces hiroshimensis	AB249922.1
Streptomyces humidus	DQ442508.1
Streptomyces humiferus	AF503491.1
Streptomyces labedae	AB184704.1
Streptomyces lanatus	AB184845.1
Streptomyces laurentii	AJ781342.1
Streptomyces lavendofoliae	AJ781336.1
Streptomyces lavendulocolor	DQ442516.1
Streptomyces leeuwenhoekii	EU551711.2
Streptomyces lienomycini	AJ781353.1
Streptomyces lilanicus	AB184819.1
Streptomyces longwoodensis	AB184580.1
Streptomyces lydicus	Y15507.1
Streptomyces macrosporus	Z68099.1
Streptomyces marinus	AB473554.1
Streptomyces mauvecolor	AB184532.1
Streptomyces megasporus	AB184617.1
Streptomyces melanogenes	AB184222.1
Streptomyces microflavus	AY999869.1
Streptomyces monomycini	DQ445790.1
Streptomyces mutabilis	EF178679.1
Streptomyces niger	AJ621607.2
Streptomyces nodosus	AF114033.1:1001-2528
Streptomyces olivochromogenes	AY094370.1
Streptomyces pactum	AB184398.1
Streptomyces panacagri	AB245388.1
Streptomyces pilosus	AB184161.1
Streptomyces polymachus	KM229363.1
Streptomyces prunicolor	DQ026659.1
Streptomyces rameus	AY999821.1
Streptomyces ramulosus	DQ026662.1
Streptomyces rangooensis	AB184295.1
Streptomyces rapamycinicus	EF408733.1

Organism	**Accession number**
Streptomyces rosealbus	AY222322.1
Streptomyces ruber	AB184604.1
Streptomyces rubidus	AY876941.1
Streptomyces rubrisoli	KC137299.1
Streptomyces rubrogriseus	AB184681.1
Streptomyces sampsonii	D63871.1
Streptomyces sannanensis	AB184579.1
Streptomyces scabiei	D63862.1
Streptomyces scabrisporus	AB030585.1
Streptomyces septatus	AY999925.1
Streptomyces showdoensis	AB184389.1
Streptomyces subrutilis	X80825.1
Streptomyces tacrolimicus	FN429653.1
Streptomyces tendae	D63873.1
Streptomyces tricolor	AB184687.1
Streptomyces tritolerans	DQ345779.2
Streptomyces tsukubensis	AB217600.1
Streptomyces venezuelae	AB045890.1
Streptomyces violaceolatus	AF503497.1
Streptomyces violaceorectus	AB184314.1
Streptomyces violaceoruber	AF503492.1
Streptomyces violaceorubidis	AJ781374.1
Streptomyces violaceus	AB184315.1
Streptomyces violaceusniger	AB184420.1
Streptomyces violascens	AY999737.1
Streptomyces violatus	AJ399480.1
Streptomyces virens	DQ442554.1
Streptomyces virginiae	AB184175.1
Streptomyces xantholiticus	AB184349.1

APPENDIX 4

Mean size of EVs produced by wildtype *S. nodosus* and *S. nodosus* MAΩ*hyg*

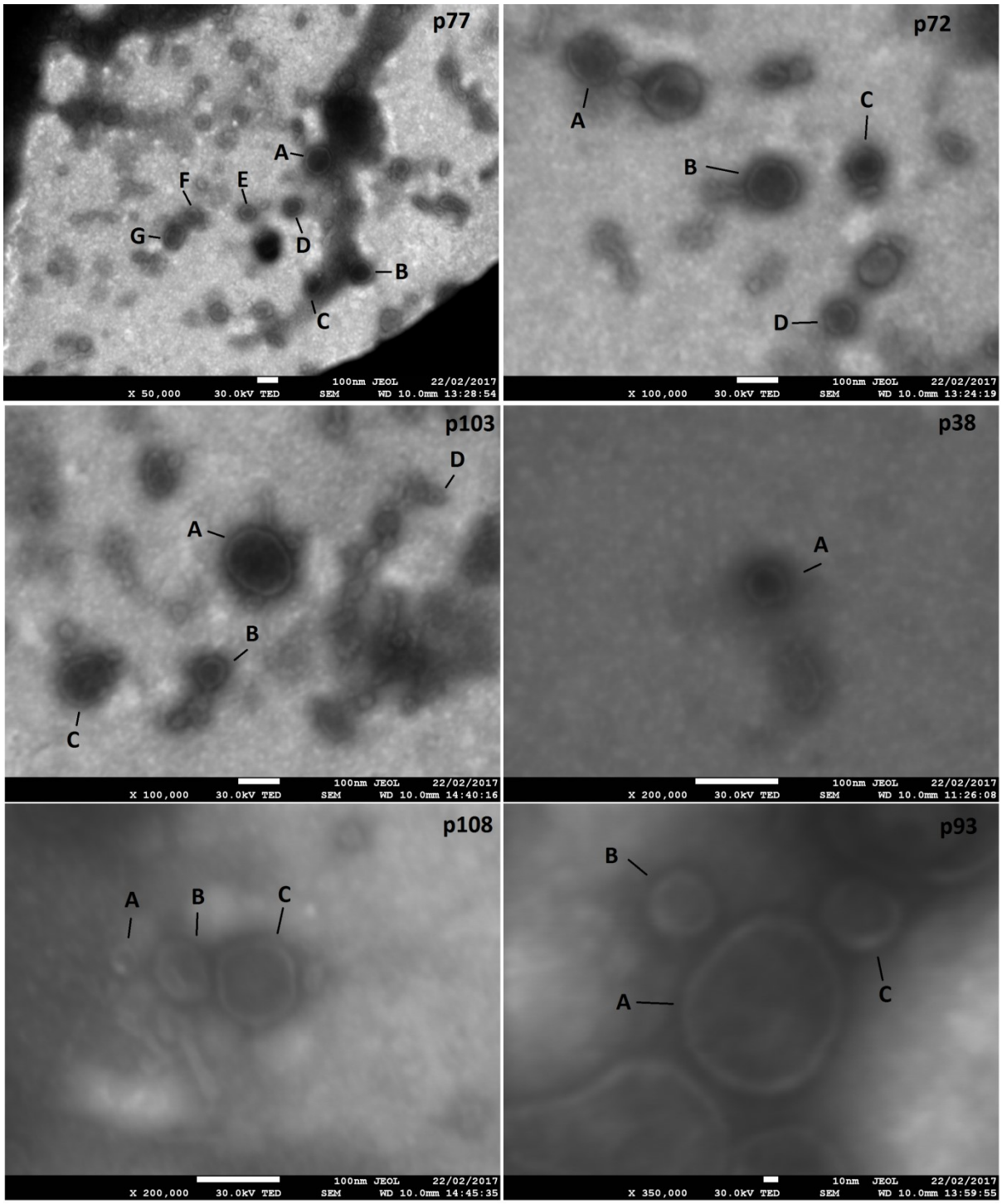

Figure A4.1: Extracellular vesicles isolated from *S. nodosus* culture broth. Images taken at the AMCF WSU using a JEOL 7001F SEM equipped with a TED detector in STEM mode at magnifications from 50,000 x - 350,000 x .

Table A4.1: Diameters of randomly selected *S. nodosus* vesicles

Photo	Vesicle	Vesicle diameter (nm)
p77	A	137
p77	B	104
p77	C	83
p77	D	80
p77	E	70
p77	F	70
p77	G	96
p72	A	113
p72	B	119
p72	C	84
p72	D	74
p103	A	151
p103	B	66
p103	C	128
p103	D	27
p38	A	50
p108	A	34
p108	B	62
p108	C	98
p93	A	111
p93	B	46
p93	C	52

n=22 average vesicle diameter = 84.31 ± 33.42

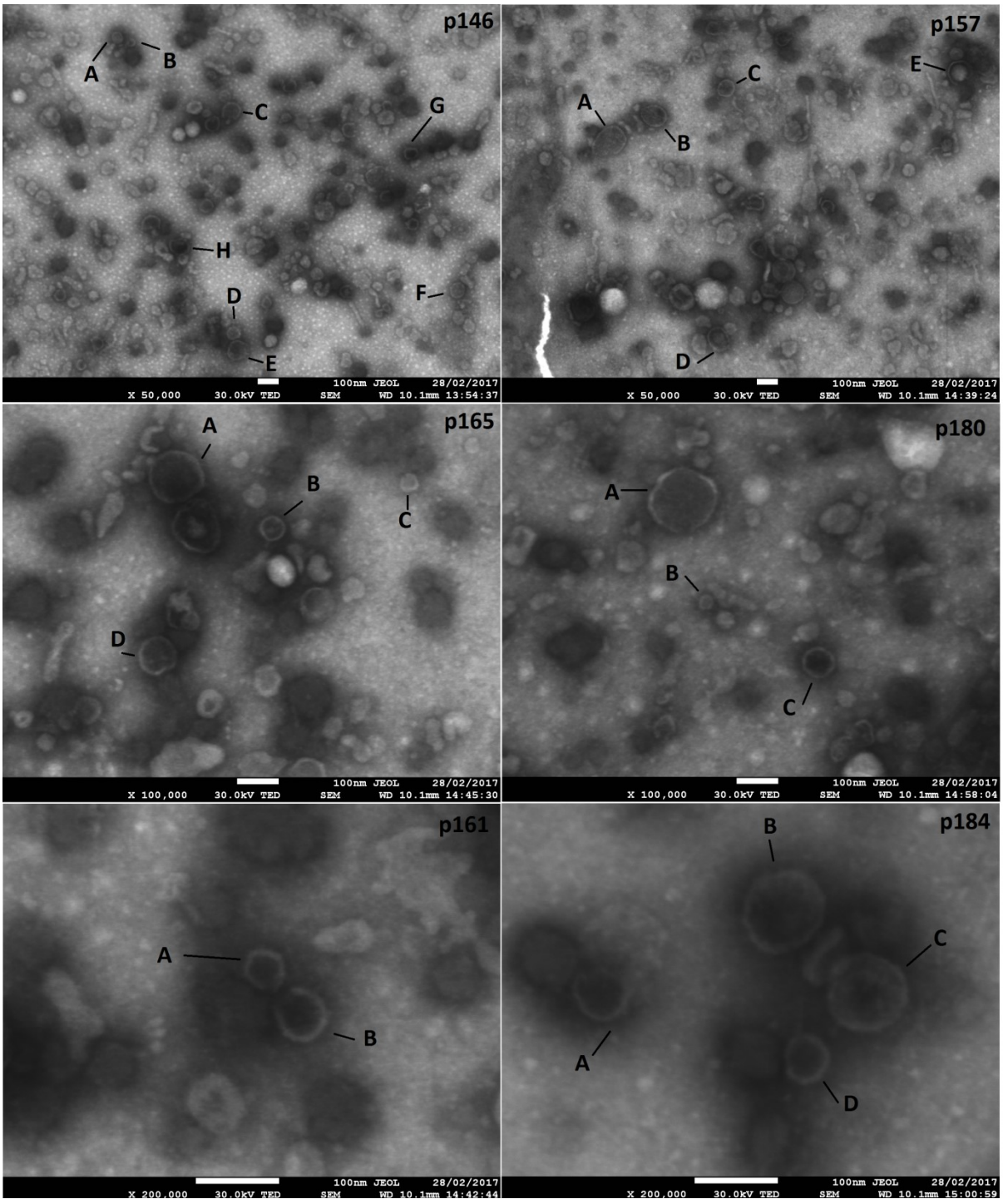

Figure A4.2: Extracellular vesicles isolated from *S. nodosus* MAΩ*hyg* culture broth. Images taken at the AMCF WSU using a JEOL 7001F SEM equipped with a TED detector in STEM mode at magnifications from 50,000 x - 200,000 x .

Table A4.2: Diameters of randomly selected *S. nodosus* MAΩ*hyg* vesicles

Photo	Vesicle	Vesicle diameter (nm)
p146	A	54
p146	B	43
p146	C	91
p146	D	67
p146	E	94
p146	F	74
p146	G	70
p146	H	100
p157	A	157
p157	B	122
p157	C	83
p157	D	104
p157	E	113
p165	A	127
p165	B	59
p165	C	43
p165	D	90
p180	A	163
p180	B	35
p180	C	79
p161	A	50
p161	B	60
p184	A	64
p184	B	100
p184	C	93
p184	D	53

n=26 average vesicle diameter = 84.15 ± 33.39